

Atropisomer Control in Macrocyclic Factor VIIa Inhibitors

Peter W Glunz, Luciano Mueller, Daniel L. Cheney, Vladimir Ladziata, Yan Zou,
Nicholas R. Wurtz, Anzhi Wei, Pancras C Wong, Ruth R. Wexler, and E. Scott Priestley

J. Med. Chem., **Just Accepted Manuscript** • DOI: 10.1021/acs.jmedchem.6b00244 • Publication Date (Web): 25 Mar 2016

Downloaded from <http://pubs.acs.org> on March 29, 2016

Just Accepted

“Just Accepted” manuscripts have been peer-reviewed and accepted for publication. They are posted online prior to technical editing, formatting for publication and author proofing. The American Chemical Society provides “Just Accepted” as a free service to the research community to expedite the dissemination of scientific material as soon as possible after acceptance. “Just Accepted” manuscripts appear in full in PDF format accompanied by an HTML abstract. “Just Accepted” manuscripts have been fully peer reviewed, but should not be considered the official version of record. They are accessible to all readers and citable by the Digital Object Identifier (DOI®). “Just Accepted” is an optional service offered to authors. Therefore, the “Just Accepted” Web site may not include all articles that will be published in the journal. After a manuscript is technically edited and formatted, it will be removed from the “Just Accepted” Web site and published as an ASAP article. Note that technical editing may introduce minor changes to the manuscript text and/or graphics which could affect content, and all legal disclaimers and ethical guidelines that apply to the journal pertain. ACS cannot be held responsible for errors or consequences arising from the use of information contained in these “Just Accepted” manuscripts.

Atropisomer Control in Macrocyclic Factor VIIa Inhibitors

Peter W. Glunz, Luciano Mueller, Daniel L. Cheney, Vladimir Ladziata, Yan Zou,† Nicholas R. Wurtz,
Anzhi Wei, Pancras C. Wong, Ruth R. Wexler and E. Scott Priestley*

Bristol-Myers Squibb Research & Development, 311 Pennington-Rocky Hill Road, Pennington, NJ
08534.

**RECEIVED DATE (to be automatically inserted after your manuscript is accepted if required
according to the journal that you are submitting your paper to)**

Running title: Atropisomerism in FVIIa macrocycles.

†Deceased. Date of death: 03/21/2014.

ABSTRACT. Incorporation of a methyl group onto a macrocyclic FVIIa inhibitor improves potency 10-fold, but is accompanied by atropisomerism due to restricted bond rotation in the macrocyclic structure, as demonstrated by NMR studies. We designed a conformational constraint favoring the desired atropisomer in which this methyl group interacts with the S2 pocket of FVIIa. A macrocyclic inhibitor incorporating this constraint was prepared and demonstrated by NMR to reside predominantly in the desired conformation. This modification improved potency 180-fold relative to the unsubstituted, racemic macrocycle and improved selectivity. An X-ray crystal structure of a closely related analog in the FVIIa active site was obtained and matches the NMR and modeled conformations, confirming that this conformational constraint does indeed direct the methyl group into the S2 pocket as designed. The

1
2 resulting rationally designed, conformationally stable template enables further optimization of these
3
4 macrocyclic inhibitors.
5
6
7
8
9

10 **Introduction**

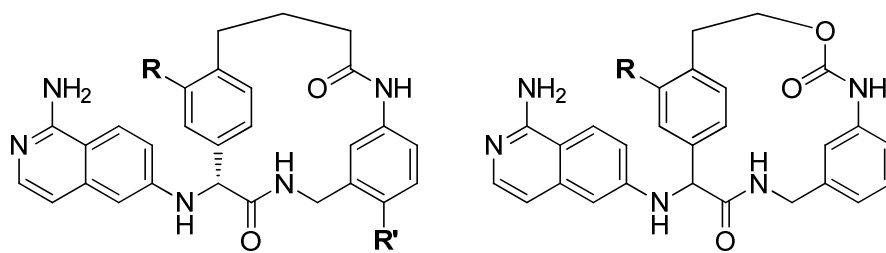
11
12 Atropisomers are stereoisomers with axial chirality arising from restricted rotation around a single
13 bond. Ōki has proposed a minimum 1000 second half-life criterion for atropisomers, sufficient
14 conformational stability for chemical separation of the individual conformers.¹ Often atropisomerism is
15 observed in biaryl systems in which steric hindrance, usually at the ortho position, prevents free rotation
16 of the two aryl rings.² Constraining a molecule into a cyclic structure can also give rise to
17 atropisomerism as in some natural products. Complestatin incorporates a phenyl-indole linkage into a
18 17-membered macrocycle, which restricts rotation leading to atropisomers.³ Similarly, Vancomycin
19 contains a pair of atropisomeric biaryl ethers constrained into the CD and DE macrocyclic ring systems,
20 as well as an atropisomeric biaryl bond connecting the AB ring.⁴
21
22
23
24
25
26
27
28
29
30
31
32
33

34
35 In drug discovery, the presence of atropisomers can complicate synthesis, analytical characterization,
36 and evaluation of biological and ADME properties, and introduces development challenges.⁵ All of
37 these issues can be further exacerbated by equilibration of the atropisomers. Strategies for addressing
38 atropisomers in drug discovery include introducing symmetry to remove the chiral axis, reducing steric
39 hindrance to allow for rapid interchange of rotameric states, or stabilization of the atropisomer by either
40 increasing steric hindrance to prevent equilibration or introducing an additional stereochemical feature
41 to favor the desired atropisomeric state.⁶
42
43
44
45
46
47
48
49
50

51
52 Macrocyclic molecules have gained attention in drug design for their ability to present diverse
53 functionality and stereochemical complexity in a conformationally defined structure.⁷ Recently, we have
54 reported utilizing macrocyclization to restrict a FVIIa inhibitor into its bioactive conformation identified
55
56
57
58
59
60

1 from the enzyme-bound X-ray crystal structure of an uncyclized inhibitor.⁸ The bound X-ray crystal
2 structure and enhanced potency of the macrocycle relative to the uncyclized inhibitor provided evidence
3 that the desired conformation was attained.
4
5
6
7

8
9
10 In this macrocyclic chemotype, we sought to exploit an interaction with the S2 pocket of FVIIa, an
11 important interaction employed in many FVIIa inhibitors.⁹ Incorporation of a methyl group at the 3-
12 position of the core phenyl ring of macrocycle **2** and a closely related carbamate-linked macrocycle **5**
13 improved potency 5- and 10-fold, respectively, relative to unsubstituted macrocycles **1** and **4**. However,
14 NMR spectra of these macrocycles showed apparent conformational heterogeneity, due to
15 atropisomerism arising from restricted rotation of the unsymmetrically substituted phenyl ring
16 constrained in a macrocycle. In addition to the complexity observed in the NMR spectra of these and
17 related macrocyclic compounds, the atropisomers were oftentimes separable by chromatography, but
18 equilibrated prior to analysis. Thus, this conformational heterogeneity confounded isolation, structural
19 characterization, and purity assessment of macrocycles bearing this P2 substituent. These effects of
20 atropisomerism introduced a roadblock in optimizing this series of macrocycles. In addition, the
21 observed ~1:1 ratio of conformers suggested that the methyl group was oriented to engage the S2 pocket
22 50% of the time and thus is not fully contributing to binding affinity and selectivity for FVIIa. In this
23 paper, we characterize the conformational heterogeneity of these macrocycle systems, including the
24 interchange of their conformers by NMR. We then report a structure-based design approach to overcome
25 the atropisomer issue preventing the advancement of this series through conformational control of the
26 macrocyclic phenylglycine core to a single atropisomer, while exploiting fully the S2 interaction.
27
28
29
30
31
32
33
34
35
36
37
38
39
40
41
42
43
44
45
46
47
48
49
50
51
52
53
54
55
56
57
58
59
60



1, R = H, R' = SO₂Et, TF/FVIIa K_i = 8.0 nM 4, R = H, TF/FVIIa K_i = 510 nM
 2, R = Me, R' = SO₂Et, TF/FVIIa K_i = 1.6 nM 5, R = Me, TF/FVIIa K_i = 46 nM
 3, R = H, R' = H, TF/FVIIa K_i = 400 nM

Figure 1. Macrocyclic FVIIa inhibitors.

Results and Discussion

NMR characterization of macrocycle 3. The solution-phase structure of the unsubstituted, amide-linked macrocycle **3** in DMSO was determined by NMR (Figure 2) and was found to be similar to the crystal structure of the same molecule bound in FVIIa.⁸ Rapid interconversion (on the NMR time scale) of the hydrocarbon chain in the macrocycle between the chair and saddle conformers was observed. Inspection of the electron-density map of the crystal structure of macrocycle **3** suggested that both the saddle and chair conformers may be populated as well in the FVIIa-bound state.

The assignment of resolved NMR signals for the P2 phenyl protons made it possible to monitor the rotation of this ring, and thus the exchange of rotameric states. Via a series of NOE-exchange experiments at temperatures ranging from 22 to 49 °C, the lifetimes of the rotameric states were measured and ranged from 58 seconds ($t_{1/2} = 40$ s) to 9 seconds ($t_{1/2} = 6$ s) at 22 and 49 °C, respectively (see Supplemental Materials for further details). This corresponds to an activation barrier of ~12.4 kcal/mol.¹⁰ Despite the lack of substitution, the slow interchange of the phenyl ring, on the order of one minute at 22 °C, shows that rotation of the phenyl ring is considerably restricted by incorporation into the macrocyclic structure even in the absence of an additional ring substituent. These results for the unsubstituted macrocycle **3** are consistent with apparent atropisomers observed for methyl-substituted macrocycle **2**.

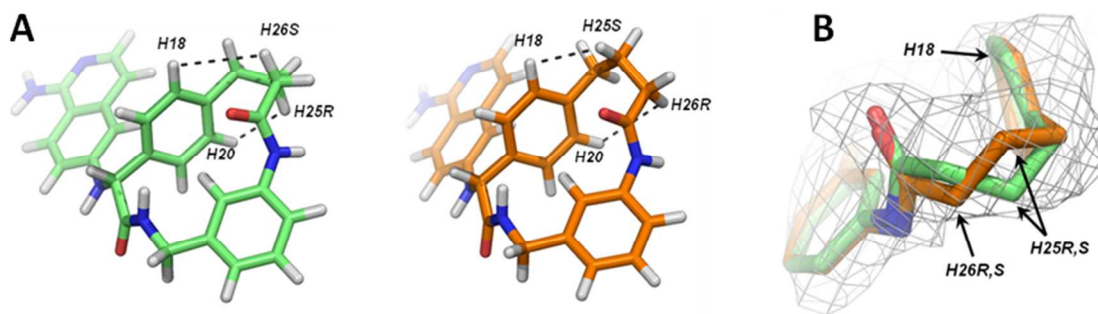
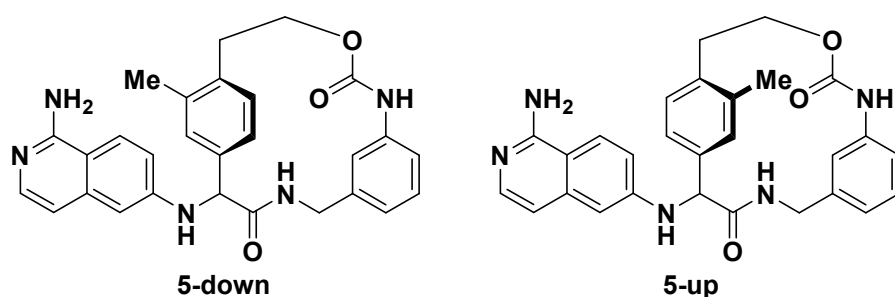


Figure 2. A. Representative NMR solution structures of macrocycle **3**, saddle conformation (green) and chair conformation (orange). B. Superposition of the same NMR conformers with electron density map (initial Fo-Fc at 3 RMSD) of the crystal structure of macrocycle **3** bound to factor VIIa suggests that averaging of the saddle and chair conformers takes place in the enzyme-bound form as well.¹¹

NMR Characterization of macrocycle 5. The conformational properties of methyl-substituted, carbamate-linked macrocycle **5** were studied by NMR. The observed structural heterogeneity gave rise to most protons producing two resonances of comparable intensity. For example, two peaks of almost equal intensities are evident for the P2 methyl group (2.26 and 2.40 ppm), corresponding to the up and down orientations of the P2 methyl relative to the plane of the macrocycle as depicted in Figure 3. A modified NOE-difference experiment was employed to prove that the observed peak splittings were due to a pair of slowly interconverting conformers. Ring-flip rates could be extracted from NOE-difference spectra at a series of temperatures. Arrhenius fit of exchange rates produced an activation energy of the phenyl ring flip of 12.4 kcal/mol for compound **5** (for details see Supplemental Materials). This activation energy for ring flip is remarkably similar to the previously determined activation energy in compound **3**. The primary difference in the Arrhenius fits of NOESY data in compounds **3** and **5** were the exchange factors A, which were 13.5 in compound **5** and 17.2 in compound **3**. This difference in exchange rate accounted for the much slower phenyl ring flips in compound **5** at room temperature which produced an estimated life time of a rotameric state in the macrocyclic ring of compound **5** of

1
2 approximately 2600 seconds ($t_{1/2} = \sim 1800$ s). Thus, the modified NOE difference data demonstrate that
3
4 the rotation of the phenyl group in **5** is restricted in the macrocycle ring and at room temperature this
5
6 substituted phenyl group does not readily equilibrate, leading to the observed atropisomerism. The
7
8 atropisomeric stability of macrocycle **5**, and related structures, is moderate; conformations neither
9
10 rapidly convert nor retain long-term stereochemical integrity. This characteristic, referred to as Class 2
11
12 atropisomerism, is a potential liability in drug development due to interconversion of stereoisomers on
13
14 the timeframe of isolation, analytical characterization, assaying and storage.⁵ Thus, we considered this
15
16 conformational heterogeneity a hindrance to advancing this chemotype.
17
18
19
20
21
22
23
24



36 Figure 3. Depictions of the two atropisomers of the P2 phenyl in macrocycle **5**: C-3 methyl down (left)
37 and C-3 methyl up (right) relative to the plane of the macrocycle. In the NOE-difference experiments the
38 methyl group in one conformer is irradiated and the exchange peak is measured.
39
40
41
42
43
44

45 **Computational studies to design conformational constraint to enforce desired atropisomer.** We
46 set out to design a means to constrain the macrocycle inhibitor to a single, desired atropisomer, and
47 hypothesized that given its close proximity to the P2 phenyl, substitution on the carbamate linker might
48 direct the 3-position methyl to the desired down orientation. Computationally, we examined the effect of
49 methyl substitution and its stereochemistry at both the benzylic and homobenzylic positions. To simplify
50 the quantum chemical calculations, we reduced the P1 aminoisoquinoline to phenyl and restricted our
51 attention to rotational states of the P2 phenyl (**6-10**, Figure 4), where we estimated the relative energy
52
53
54
55
56
57
58
59
60

1 costs of positioning the 3-position methyl down or up. The two rotamers of **6** (the truncated version of
2 macrocycle **5** lacking substitution on the carbamate linker) showed similar calculated energies,
3
4
5
6 consistent with the equal rotameric populations observed in the solution NMR spectrum of macrocycle
7
8
9 **5**. Substitution at the benzylic position had a larger effect on the calculated energy difference between
10
11 the rotameric states, with the stereochemistry of the methyl substituent determining the rotameric
12
13 preference. The 3-position methyl group pointing down, which represents the desired atropisomer, is
14
15 favored by 1.9 kcal/mol in the *R*-stereoisomer (**7**). In contrast, the *S*-stereoisomer (**8**) favored the methyl
16
17 group pointing up, the undesired atropisomer, by 3.7 kcal/mol. Substitution at the homobenzylic position
18
19 had a smaller calculated effect on the rotameric preference of the P2 phenyl. The *R*-stereoisomer (**9**)
20
21 weakly favored (0.8 kcal/mol) the desired atropisomer, whereas the *S*-stereoisomer (**10**) weakly favored
22
23 (0.5 kcal/mol) the undesired atropisomer. Overall, these calculations suggested that an *R*-methyl
24
25
26
27
28 substituent at the benzylic position of the carbamate linker would stabilize the desired P2 atropisomer.
29
30
31
32
33
34
35
36
37
38
39
40
41
42
43
44
45
46
47
48
49
50
51
52
53
54
55
56
57
58
59
60

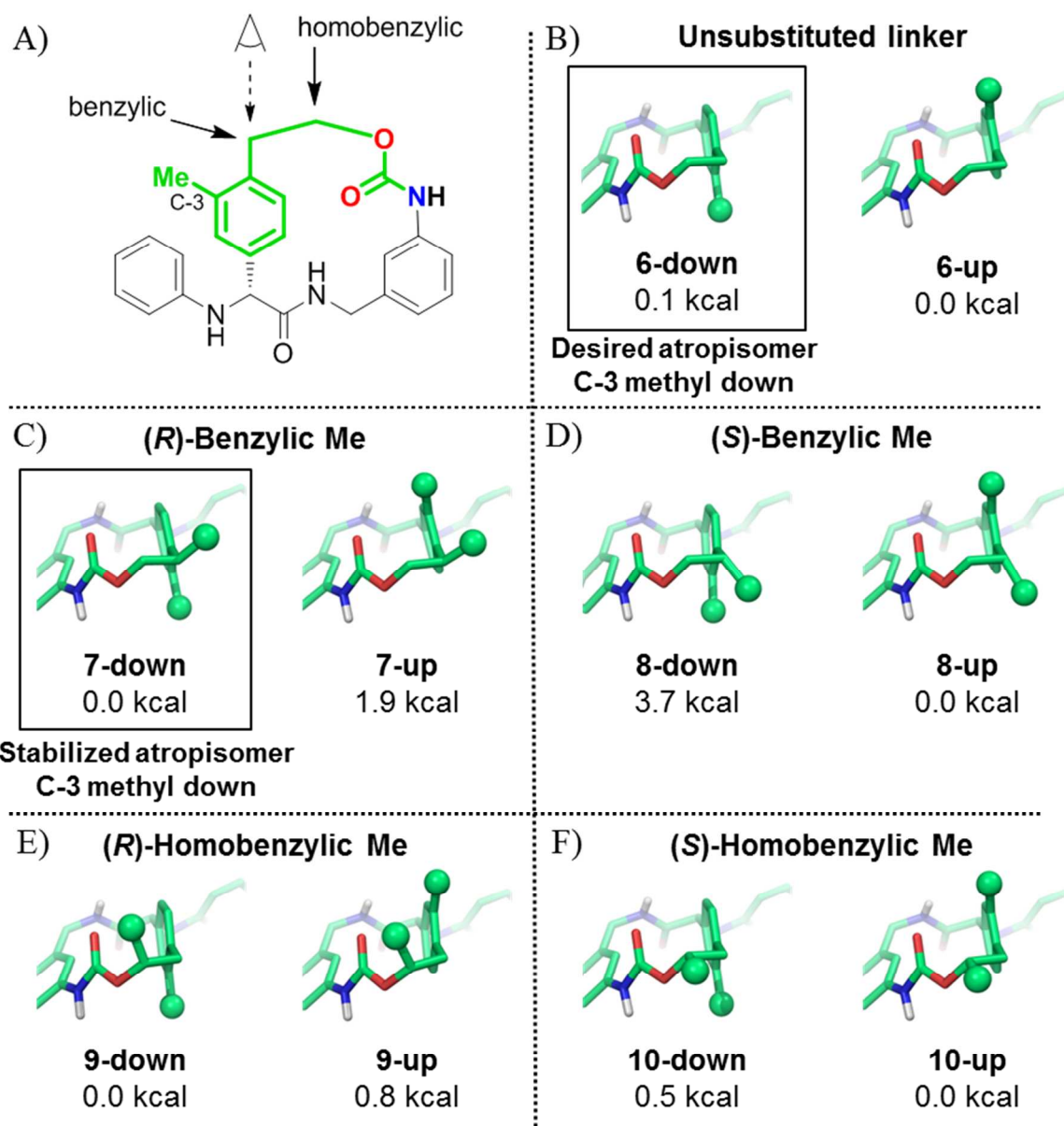
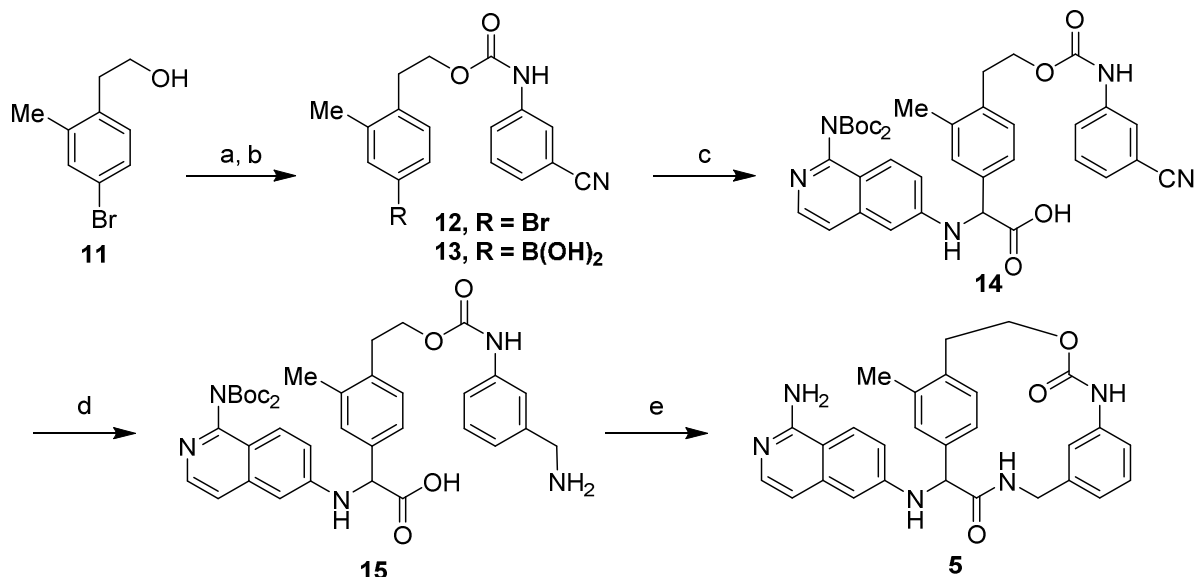


Figure 4. Energies for rotameric states of the P2 phenyl (C-3 methyl is oriented either down or up relative to the macrocycle ring) in truncated model systems **6-10**, panels B-F. (*R*)-Benzylic methyl (panel C) favors the desired, methyl-down conformation by 1.9 kcal/mol. The aminoisoquinoline group was replaced with a phenyl moiety to simplify calculations. Molecular graphics were generated with the program Pymol.¹¹

Chemistry. The synthesis of macrocycle **5** with methyl substitution on the P2 phenyl is shown in Scheme 1. Carbamate **12** was prepared by coupling of phenethanol **11** and 3-isocyanatobenzonitrile. Conversion of the resultant bromo intermediate **12** to the boronic acid **13** was accomplished by Miyaura

borylation with bis(neopentyl glycolato)diboron, followed by hydrolysis. Petasis three-component coupling¹² between boronic acid **13**, *tert*-butyl *N*-(6-aminoisoquinolin-1-yl)-*N*-[(*tert*-butoxy)carbonyl]carbamate,¹³ and glyoxylic acid monohydrate assembled the phenylglycine core (**14**). Reduction of the nitrile functionality afforded amino intermediate **15**, which served as the macrocyclization precursor. Macrocyclization was accomplished via syringe-pump addition of **15** into PyBop, DMAP and TEA, which after TFA deprotection afforded **5**.

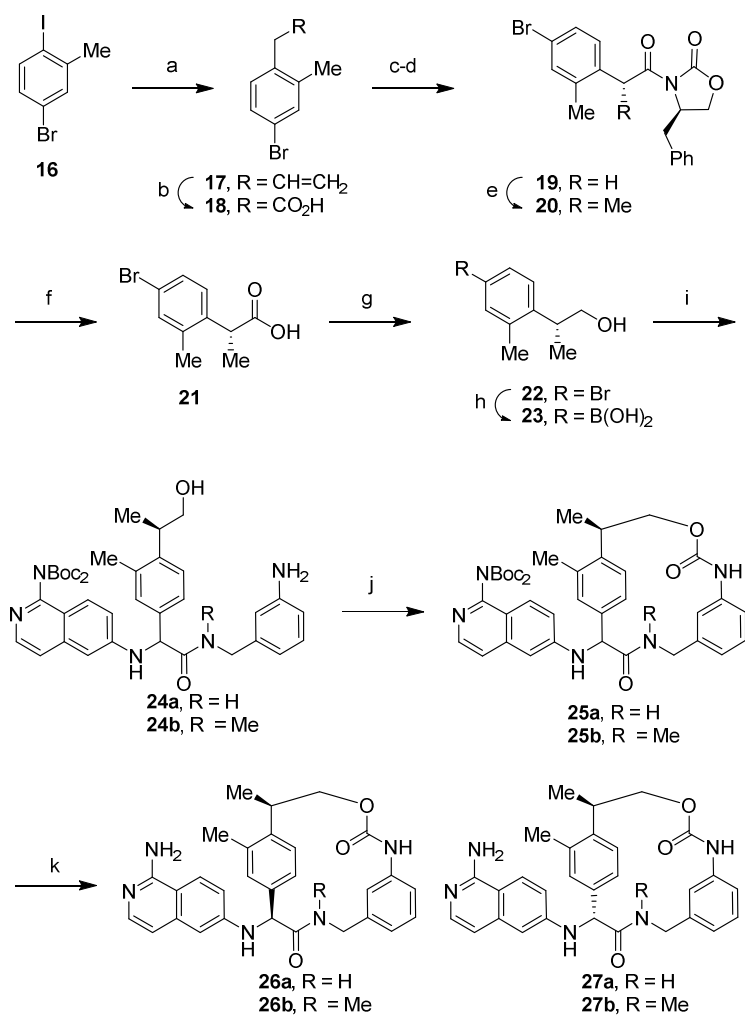
Scheme 1. Synthesis of macrocycle **5**^a

^aReagents and conditions: (a) NaH, THF; 3-isocyanatobenzonitrile, 62 %; (b) bis(neopentyl glycolato)diboron, Pd(dppf)Cl₂, DMSO, 64 %; (c) *tert*-butyl *N*-(6-aminoisoquinolin-1-yl)-*N*-[(*tert*-butoxy)carbonyl]carbamate, glyoxylic acid monohydrate, CH₃CN, DMF, 34 %; (d) H₂, 10% Pd-C, MeOH, 45 %; (e) Syringe-pump addition into PyBop, TEA, DMAP; TFA, 42 %.

Macrocycles **26** and **27**, containing the (*R*)-benzylic methyl, were synthesized as shown in Scheme 2. Allylation of iodobenzene **16**, followed by Ru(III)-catalyzed oxidation afforded phenylacetic acid **18**. Treatment of this acid with oxalyl chloride afforded the acid chloride, which was coupled with (*R*)-

1
2 benzyloxazolidin-2-one chiral auxiliary to yield imide **19**. Alkylation of **19** with methyl iodide afforded
3
4 intermediate **20**. Cleavage of the chiral auxiliary, followed by reduction of the resultant acid
5
6 functionality (**21**), provided alcohol **22**. Subjecting this intermediate to Miyaura borylation conditions,
7
8 followed by hydrolysis, afforded boronic acid **23**. A one-pot Petasis three-component coupling/amide
9
10 coupling afforded the macrocyclization precursor **24** in a single step. In this procedure, boronic acid **23**,
11
12 *tert*-butyl *N*-(6-aminoisoquinolin-1-yl)-*N*-[(*tert*-butoxy)carbonyl]carbamate, and glyoxylic acid
13
14 monohydrate are heated to generate the phenylglycine derivative. To this reaction mixture, is added 3-
15
16 (aminomethyl)aniline and BOP to accomplish amide formation, yielding aminoalcohol **24**. Reaction of
17
18 **24** with phosgene, followed by syringe-pump addition of the activated species into a solution of TEA,
19
20 closed the macrocycle to give **25**. Separation of diastereomers via chiral chromatography and
21
22 deprotection afforded diastereomeric macrocycles **26** and **27**.
23
24
25
26
27
28
29
30
31

32 Scheme 2. Synthesis of macrocycles **26a,b** and **27a,b**^a
33
34
35
36
37
38
39
40
41
42
43
44
45
46
47
48
49
50
51
52
53
54
55
56
57
58
59
60



36 ^aReagents and conditions: (a) *i*-PrMgCl, LiCl, CuCN, THF; allyl bromide, 100 %; (b) RuCl₃, NaIO₄,
 37 CCl₄, H₂O, 85 %; (c) (COCl)₂, CH₂Cl₂; (d) (*R*)-benzyloxazolidin-2-one, BuLi, THF, 78 %, 2 steps; (e)
 38 NaHMDS, THF; MeI, 65 %; (f) LiOH, H₂O₂, THF, 98 %; (g) BH₃, THF, 97 %; (h) 5,5,5',5'-tetramethyl-
 40 2,2'-bi(1,3,2-dioxaborinane), Pd(dppf)Cl₂, KOAc, DMSO, 71 %; (i) *tert*-butyl *N*-(6-aminoisoquinolin-1-
 41 yl)-*N*-[(*tert*-butoxy)carbonyl]carbamate, glyoxylic acid monohydrate, CH₃CN/DMF; 3-
 42 (aminomethyl)aniline or 3-((methylamino)methyl)aniline, BOP, TEA (**24a**, 55 %; **24b**, 51 %); (j)
 43 phosgene, CH₃CN, DCM, DMPU; syringe pump addition into TEA, DCM, (**25a**, 41 %; **25b**, 49 %); (k)
 44 separation of diastereomers; TFA, (**26a**, 41 % and **27a**, 37 %; **26b**, 46 % and **27b**, 37 %).

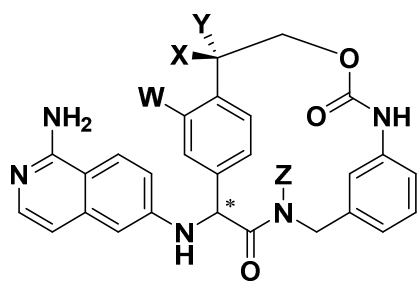
53 **TF/FVIIa activity of substituted analogs.** The substituted macrocycles were tested for inhibition of
 54 TF/FVIIa and a panel of serine proteases, and the data are summarized in Table 1. Unsubstituted
 55 macrocycle **4** has a FVIIa K_i of 510 nM, with similar inhibitory activity against FXa and modest
 56
 57
 58
 59
 60

1
2 selectivity versus the other serine proteases. Introduction of the 3-position methyl substituent (**5**)
3
4 improves potency 10-fold. Introduction of a benzylic methyl group with *R*-stereochemistry (**28**)
5
6 improves potency 4-fold relative to **4**; both compounds are 1:1 mixtures of stereoisomers at the
7
8 phenylglycine α -center. *R*-stereochemistry at the benzylic position is 10-fold more potent than the *S*-
9
10 stereochemistry (**28** vs. **29**). The observed preference for the *R*-methyl substituent is fortunate as it
11
12 suggested that we might not only control the atropisomeric preference for the subsequent substitution of
13
14 the P2-phenyl group as predicted in our calculations, but might also derive an additional binding
15
16 interaction from this group. Combining these two substituents, the 3-position and benzylic methyl
17
18 groups, affords the potent inhibitor **27a** with TF/FVIIa $K_i = 1.4$ nM. The phenylglycine C- α
19
20 diastereoisomer **26a** is very weakly active ($K_i = 4510$ nM), as is consistent with previously prepared
21
22 macrocycles **1-3**,⁸ in which activity resides in the *R*-stereoisomer. *N*-methylation of the amide (**27b**)
23
24 provides a compound with similar activity relative to the secondary amide **27a**. Macrocycle **27b** is
25
26 significantly more selective against FXa, FXIa, thrombin and trypsin than the unsubstituted macrocycle
27
28 **4** and singly methyl-substituted macrocycles **5** and **28**. Much of this >1000-fold selectivity is due to
29
30 improvement in activity against FVIIa. These macrocyclic inhibitors lacking substitution on the benzyl
31
32 amide portion, which points to the S1' pocket, are consistently potent against tissue kallikrein.
33
34 Selectivity against this serine protease family is important, as it is implicated in cancer-related
35
36 processes¹⁴ and many other physiological functions.¹⁵ The unsubstituted macrocycle **4** favors tissue
37
38 kallikrein by 15 fold relative to FVIIa. The optimized macrocycle **27b** improves to 28-fold selective
39
40 against tissue kallikrein, owing to its increased potency against FVIIa. Substitution on the benzylamide
41
42 moiety to interact with the S1' pocket provides a means to improve tissue kallikrein selectivity, which
43
44 will be presented separately.¹⁶
45
46
47
48
49
50
51
52
53
54

55 Macrocycle **27a** is 16-fold more potent than methyl-substituted macrocycle **5** and 180-fold more
56
57 potent than the unsubstituted macrocycle **4**, after accounting for stereochemistry. Overall, this observed
58
59
60

180-fold increase in potency is larger than the combined 40-fold increase in potency predicted from the individual contributions of each of the two methyl substituents: 3-position methyl (10-fold, **5** vs. **4**) and *R*-benzylic methyl (4-fold, **28** vs. **4**). This result suggests there may be cooperativity of these two interactions.

Table 1. SAR for substituted macrocycles.^a



Cmpd	Phg Stereochem	W	X	Y	Z	Ki (nM)					
						TF/FVIIa	FXa	FXIa	thrombin	trypsin	tissue kall
4	R/S	H	H	H	H	510	610	5700	>13000	3500	35
5	R/S	Me	H	H	H	46	2600	10800	>13000	4500	6
28	R/S	H	Me	H	H	140	4500	9100	4700	>6200	25
29	R/S	H	H	Me	H	1450	6800	>11000	7400	>6200	4
26a	R	Me	Me	H	H	4510	>13300	>14200	>11500	>10000	31
26b	R	Me	Me	H	Me	1150	>13300	>14200	>11500	>10000	154
27a	S	Me	Me	H	H	1.4	>13300	>14200	>11500	>10000	25
27b	S	Me	Me	H	Me	1.3	>13300	>14200	>11500	>10000	36

^a Ki values were averaged from two experiments. TF/FVIIa assays were performed with recombinant human enzyme, while other enzyme assays were performed with purified human enzymes. All assays were run at 25 °C except tissue kallikrein 1, which was run at 37 °C. Detailed descriptions of the enzyme assay protocols have been reported.¹⁷ Tissue kall = tissue kallikrein 1.

1
2
3
4
5
6
7
8
9
10
11
12
13
14
15
16
17
18
19
20
21
22
23
24
25
26
27
28
29
30
31
32
33
34
35
36
37
38
39
40
41
42
43
44
45
46
47
48
49
50
51
52
53
54
55
56
57
58
59
60

NMR structure of macrocycle 27a. The NMR solution structure of **27a** in DMSO was determined by dynamic simulated annealing in XPLOR starting from a randomized 3D-structure of **27a**, using 28 distance restraints (Figure 5). The structure shows predominantly a single conformation for the macrocyclic ring system, suggesting that the benzylic methyl group in fact restricts the unsymmetrically substituted phenylglycine phenyl to a single atropisomer. ¹H-NMR of **27a** in 90% aqueous/10% DMSO shows a single macrocycle conformation and similar chemical shift and J-coupling constant data when compared to 100% DMSO NMR data (see Supporting Information) suggesting preservation of the solution structure in an aqueous environment. This conformational control observed for **27a** is in contrast to the unsubstituted-linker analog **5**, which shows a 1:1 ratio of conformations (*vide supra*). Importantly, compound **27a** in solution adopts the desired conformation in which the 3-methyl group of the phenylglycine core is pointing down relative to the plane of the macrocycle ring. In the binding site of FVIIa, this atropisomer orients the methyl group into the S2 pocket. As expected, the orientation of the isoquinoline subunit is not well defined in the NMR solution structure. The conformation of this moiety is to a large extent determined by interactions with the S1 pocket of FVIIa.

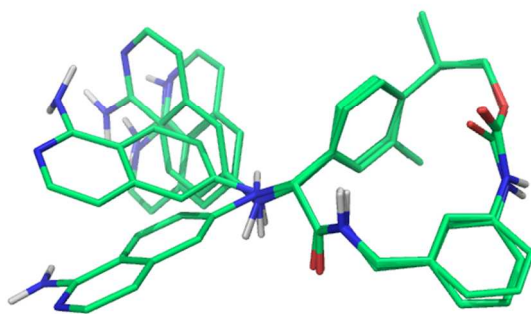


Figure 5. NMR structural studies of **27a** indicate the presence of a single dominant macrocycle conformation, placing the P2 methyl group in the desired down orientation.¹¹

X-ray structure of related macrocycle 30. The X-ray crystal structure of a closely related analog of **27a** containing the same 3-position and *R*-benzylic methyl groups (macrocycle **30**), was obtained in FVIIa (Figure 6A). Figure 6B, shows the superposition of the bound X-ray structure of **30** with the NMR solution structure of **27a** and the lowest-energy conformation from the computational studies (**7-down**, Figure 4). All three structures show very close alignment of the macrocycle core. The P2 rotamer predicted as energetically stable in our computational studies corresponded to both the dominant solution structure and the enzyme-bound structure observed in the crystal. A subsequent and broader force field-based conformational analysis was performed and estimated the bound conformation to also be the most probable in aqueous solution (74%; see Experimental Section and Supporting Information).

As shown in Figure 6A, **30** adopts the desired conformation in which the 3-position methyl group is pointing down relative to the plane of the macrocycle ring. In this orientation, the methyl group interacts with the lipophilic S2 pocket. The close similarity between the bound structure of **30** in FVIIa and the solution structure of **27a** suggests that the latter compound is also making this interaction with the S2 pocket. The increased potency of **27a** relative to the unsubstituted macrocycle **5** provides further support that this interaction is indeed formed.

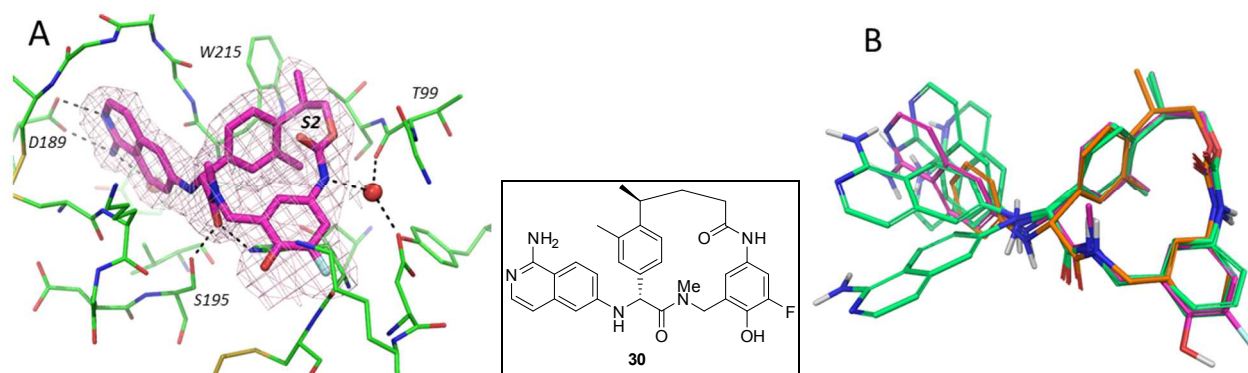


Figure 6. A. Crystallographic structure of **30** (structure shown in inset) bound in factor VIIa (2.06 Å resolution). The initial Fo-Fc electron density map is depicted within 1.5 Å of the ligand at a contour of 3.0 RMSD.¹⁸ B. Superposition of the bound conformation of **30** in factor VIIa (magenta) with the NMR

1
2 solution structures of **27a** (green) and lowest energy conformation of a truncated structure of **27a** (7-
3 **down**, see Figure 4C) in which the isoquinoline has been replaced with a phenyl (orange).¹¹
4
5
6
7
8

9 **Conclusion.** We have shown that incorporation of a methyl group in the 3-position of the
10 phenylglycine core of a macrocyclic FVIIa inhibitor improves potency 10-fold, but is accompanied by
11 atropisomerism due to restricted rotation of the phenyl group in the macrocyclic structure. Based upon
12 computational studies, we proposed that incorporating an *R*-benzylic methyl group on the linker portion
13 of the macrocycle would lock the adjacent phenyl ring of the macrocycle into the desired atropisomer in
14 which the 3-position methyl points down, interacting with the S2 pocket of FVIIa. The macrocyclic
15 inhibitor **27a** incorporating the *R*-benzylic methyl was prepared and was demonstrated by NMR to exist
16 in the desired atropisomer. The *R*-benzylic methyl group in combination with the P2-methyl group (**27a**)
17 has a significant effect on potency—180-fold relative to the unsubstituted macrocycle **4**. An X-ray
18 crystal structure of a closely related analog of **27a** in FVIIa was obtained and matches the NMR
19 determined conformation in solution as well as the modeled confirmation of **27a**. In addition, this FVIIa-
20 bound X-ray structure shows that this conformational constraint does indeed direct the 3-Me group into
21 the S2 pocket as designed. Importantly, through the addition of this conformational constraint we have
22 overcome the atropisomer issue that was hindering the advancement of this macrocyclic chemotype and
23 significantly increased potency and selectivity in the process. Furthermore, this constraint has provided a
24 rigid macrocyclic scaffold with well-defined vectors for substitution to make key interactions with the
25 FVIIa active site, enabling further optimization, which will be disclosed separately.
26
27
28
29
30
31
32
33
34
35
36
37
38
39
40
41
42
43
44
45
46
47
48
49
50
51
52

53 **Experimental Section**

54
55
56
57
58
59
60

General Methods for Chemistry. All reactions were carried out using commercial grade reagents and solvents. Solution ratios express a volume relationship, unless stated otherwise. NMR chemical shifts (δ) are reported in parts per million relative to internal TMS. Flash chromatography was carried out on ISCO CombiFlash™ systems using pre-packed silica cartridges and eluted with gradients of the specified solvents. Preparative reverse phase high pressure liquid chromatography (HPLC) was carried out on C₁₈ HPLC columns using methanol/water gradients containing 0.1% trifluoroacetic acid. Purity of all final compounds was determined to be $\geq 95\%$ by analytical HPLC using the following conditions: Method A: Waters Sunfire C18 column (3.5 μ M, 3.0 x 150 mm); Method B: Waters Xbridge Phenyl column (3.5 μ M, 3.0 x 150 mm). Eluted at 1 mL/min with a 12 min gradient from 90% solvent A to 100% solvent B (solvent A: 5% acetonitrile, 95% water, 0.05% TFA; solvent B: 95% acetonitrile, 5% water, 0.05% TFA), monitoring UV absorbance at 220 nm.

4-Bromo-2-methylphenethyl 3-cyanophenylcarbamate (12)

NaH (150 mg, 60% dispersion in oil) was added portion wise to a solution of 2-(4-bromo-2-methylphenyl)ethanol (570 mg, 2.65 mmol) in THF (26.5 mL) and the mixture was stirred for 30 min. The solution was cooled to -78°C and 3-isocyanatobenzonitrile (382 mg, 2.65 mmol) was added in one portion. The cooling bath was removed and the reaction was stirred for 2 h. Water (100 mL) was added to the reaction mixture and it was extracted with EtOAc (2X). The combined organics phase was washed with brine, dried (Na_2SO_4) and concentrated. The crude product was purified by flash chromatography (0 to 100 % EtOAc/hexanes gradient) to yield **12** (590 mg, 62 % yield) as a colorless solid. ^1H NMR (400 MHz, DMSO- d_6) δ ppm 9.97 (s, 1 H) 7.85 (s, 1 H) 7.70 (d, $J=8.1$ Hz, 1 H) 7.41 - 7.55 (m, 2 H) 7.39 (d, $J=1.8$ Hz, 1 H) 7.32 (dd, $J=8.2, 1.9$ Hz, 1 H) 7.17 (d, $J=8.3$ Hz, 1 H) 4.28 (t, $J=7.0$ Hz, 2 H) 2.92 (t, $J=7.0$ Hz, 2 H) 2.30 (s, 3 H).

4-(2-(3-Cyanophenylcarbamoyloxy)ethyl)-3-methylphenylboronic acid (13)

To a flask containing **12** (730 mg, 2.0 mmol), 5,5',5'-tetramethyl-[2,2']bi[[1,3,2]dioxaborinanyl] (496 mg, 2.2 mmol), potassium acetate (868 mg, 8.84 mmol) and Pd(dppf)Cl₂·DCM (82 mg, 0.10 mmol), was added DMSO (10 mL). The reaction mixture was degassed with three cycles of vacuum followed by argon backfill. The reaction mixture was heated for 2 h at 80 °C. The mixture was diluted with water and extracted with diethyl ether (3X). The combined organic phase was dried (MgSO₄) and concentrated. The residue was dissolved in a mixture of diethyl ether (10 mL), DCM (1 mL), and EtOAc (1 mL). Diethanolamine (210 mg, 2.0 mmol) in isopropanol (5 mL) was added, and the reaction mixture was stirred overnight at rt. The reaction mixture was concentrated, and the residue was purified by preparative HPLC to give **13** (420 mg, 64 % yield) as a brown oil. MS (ESI) *m/z* 347.1 (M+Na)⁺; ¹H NMR (400 MHz, CD₃OD) δ ppm 7.77 (s, 1 H) 7.56 (d, *J*=7.8 Hz, 1 H) 7.36 - 7.52 (m, 2 H) 7.33 (t, *J*=8.0 Hz, 1 H) 7.24 (d, *J*=7.6 Hz, 1 H) 7.11 (d, *J*=7.3 Hz, 1 H) 4.26 (t, *J*=7.1 Hz, 2 H) 2.94 (t, *J*=7.1 Hz, 2 H) 2.29 (s, 3 H).

2-(5-(Bis(*tert*-butoxycarbonyl)amino)naphthalen-2-ylamino)-2-(4-(2-(3-cyanophenylcarbamoyloxy)ethyl)-3-methylphenyl)acetic acid (14)

A solution of **13** (420 mg, 1.30 mmol), *tert*-butyl N-(6-aminoisoquinolin-1-yl)-N-[(*tert*-butoxy)carbonyl]carbamate (466 mg, 1.30 mmol) and glyoxylic acid monohydrate (143 mg, 1.30 mmol) in acetonitrile (4 mL) and DMF (0.4 mL), were heated in a microwave reactor at 100 °C for 10 min. The mixture was concentrated and the residue was purified by flash chromatography (0 to 10% MeOH in CH₂Cl₂ gradient) to afford **14** (308 mg, 34 % yield) as a tan solid. MS (ESI) *m/z* 696.15 (M+H)⁺.

1
2 **2-(4-(2-(3-(Aminomethyl)phenylcarbamoyloxy)ethyl)-3-methylphenyl)-2-(5-(bis(*tert*-**
3
4 **butoxycarbonyl)amino)naphthalen-2-ylamino)acetic acid (15)**
5
6

7 To a solution of **14** (308 mg, 0.44 mmol) in MeOH (20 mL), was added Raney Ni. The mixture was
8 degassed (evacuated and flushed with Ar), then was stirred under an atmosphere of H₂ (60 psi) for 15 h.
9
10 The mixture was filtered and concentrated, then purified via preparative HPLC to give **15** (140 mg, 45
11
12 % yield) as a yellow solid. MS (ESI) *m/z* 700.15 (M+H)⁺.
13
14
15
16
17
18
19
20

21 **2-(1-Amino-isoquinolin-6-ylamino)-20-methyl-13-oxa-4,11-diazatricyclo[14.2.2.1^{6,10}]henicosa-**
22
23 **1(19),6,8,10(21),16(20),17-hexaene-3,12-dione trifluoroacetic acid salt (5)**
24
25

26 A solution of **15** (140 mg, 0.20 mmol) in DMF (5 mL) was added dropwise over 1 h via a syringe pump
27 into a solution of PyBOP (208 mg, 0.40 mmol), DMAP (172 mg, 1.0 mmol) and DIEA (0.17 mL, 1.0
28 mmol) in DCM (50 mL) at reflux. The mixture was stirred at rt for 15 h, then was concentrated. The
29 residue was dissolved in DCM and was treated with TFA (2 mL) and H₂O (5 drops). The mixture was
30 stirred at rt for 2 h, then was concentrated. The residue was purified by preparative HPLC to afford **5** (40
31 mg, 42 % yield) as a white solid. MS (ESI) *m/z* 482.20 (M+H)⁺; HRMS (ESI) *m/z* 482.2191 (0.82 ppm);
32
33 ¹H NMR (500MHz, CD₃OD) δ 8.07 (dd, *J*=9.1, 6.1 Hz, 1H), 7.50 (s, 0.5H), 7.42 (dd, *J*=7.8, 1.8 Hz,
34 0.5H), 7.34 - 7.25 (m, 2H), 7.21 (ddd, *J*=16.4, 9.1, 2.2 Hz, 1H), 7.17 - 7.11 (m, 2H), 6.94 - 6.82 (m, 2H),
35 6.75 - 6.64 (m, 2H), 6.18 (d, *J*=14.0 Hz, 1H), 5.14 (d, *J*=8.3 Hz, 1H), 4.96 - 4.88 (m, 0.5H), 4.77 - 4.69
36 (m, 0.5H), 4.55 (br. s., 1H), 4.20 - 3.96 (m, 2H), 3.21 - 3.10 (m, 1H), 2.88 - 2.75 (m, 1H), 2.51 (s, 1.6H),
37 2.36 (s, 1.4H), ~1:1 atropisomers; Purity: 99.6% (method A), 98.7% (method B).
38
39
40
41
42
43
44
45
46
47
48
49
50
51
52
53
54
55
56

57 **1-Allyl-4-bromo-2-methylbenzene (17)**
58
59
60

1
2 To a solution of 4-bromo-1-iodo-2-methylbenzene (5 g, 16.8 mmol) in THF (100 mL) at -20 °C, was
3
4 added isopropylmagnesium chloride (2M, THF) (15 mL, 30.0 mmol). The mixture was stirred at -20 °C
5
6 for 45 min. A solution of lithium chloride (1.71 g, 40.4 mmol) and copper(I) cyanide (1.81 g, 20.21
7
8 mmol) in THF (40 mL) was added. The pale green solution was stirred for 10 min at -10 °C, then allyl
9
10 bromide (4.37 mL, 50.5 mmol) was added. The mixture was stirred at -10 °C for 10 min. The reaction
11
12 was quenched with sat. NH₄Cl. and diluted with EtOAc. The organic phase was washed with H₂O, 1N
13
14 HCl and brine. The organic phase was dried (Na₂SO₄), filtered through a 1" pad of SiO₂ and
15
16 concentrated to afford **17** (3.55 g, 100 % yield) as a pale yellow oil. ¹H NMR (400 MHz, CDCl₃) δ ppm
17
18 7.24 - 7.31 (m, 2 H) 7.00 (d, *J*=7.9 Hz, 1 H) 5.86 - 5.96 (m, 1 H) 5.07 (dd, *J*=10.1, 1.3 Hz, 1 H) 4.97 (dd,
19
20 *J*=17.1, 1.3 Hz, 1 H) 3.31 (d, *J*=6.2 Hz, 2 H) 2.26 (s, 3 H).
21
22
23
24
25
26
27
28
29

30 **2-(4-Bromo-2-methylphenyl)acetic acid (18)**

31
32 To a solution of **17** (3.55 g, 16.8 mmol) in CCl₄ (100 mL), water (150 mL) and acetonitrile (100 mL) at
33
34 rt, was added Ruthenium (III) chloride hydrate (0.523 g, 2.52 mmol) and sodium periodate (18.0 g, 84
35
36 mmol). The suspension was stirred vigorously for 2.5 h, then was diluted with H₂O and DCM. The
37
38 mixture was filtered through celite. The phases were separated. The aqueous phase was extracted with
39
40 DCM (2X). The combined organic extract was washed with H₂O and brine, dried (Na₂SO₄) and
41
42 concentrated. The resultant black solid was partitioned between Et₂O and 0.1 N NaOH. The organic
43
44 phase was extracted with H₂O, then the combined aqueous extract was acidified with 12 N HCl. The
45
46 aqueous phase was extracted with EtOAc (3X). The combined organic extract was washed with H₂O and
47
48 brine, dried (Na₂SO₄), filtered through a 1" pad of SiO₂ and concentrated to afford **18** (3.26 g, 85 %
49
50 yield) as an off-white solid. MS (ESI) *m/z* 229.2 (M+H)⁺; ¹H NMR (400 MHz, CDCl₃) δ ppm 7.35 (d,
51
52 *J*=1.8 Hz, 1 H) 7.30 (dd, *J*=8.1, 2.0 Hz, 1 H) 7.06 (d, *J*=7.9 Hz, 1 H) 3.62 (s, 2 H) 2.30 (s, 3 H).
53
54
55
56
57
58
59
60

(R)-4-Benzyl-3-(2-(4-bromo-2-methylphenyl)acetyl)oxazolidin-2-one (19)

To a solution of **18** (2.77 g, 12.1 mmol) in DCM (40 mL) at rt, were added oxalyl chloride (1.16 mL, 13.3 mmol) and DMF (0.01 mL). The mixture was stirred at rt for 2 h, then concentrated to an orange oil (acid chloride). To a solution of (*R*)-4-benzyloxazolidin-2-one (2.36 g, 13.3 mmol) in THF (40 mL) at -78 °C, was added butyllithium (1.6 M, hexane) (8.31 mL, 13.3 mmol). The mixture was stirred for 5 min, then a solution of the acid chloride (12.1 mmol) in THF (10 mL). The mixture was stirred at -78 °C for 1 h, then was quenched with sat. NH₄Cl. The mixture was diluted with EtOAc and washed with H₂O and brine, dried (Na₂SO₄) and concentrated. The crude product was purified by flash chromatography (gradient from 0 to 80% ethyl acetate/hexanes). The product was suspended in hexanes (20 mL), then the product was collected and dried in vacuo to afford **19** (3.65 g, 78 % yield) as a colorless, crystalline solid. MS (ESI) *m/z* 387.9 (M+H)⁺; ¹H NMR (400 MHz, CD₃OD) δ ppm 7.37 (d, *J*=1.7 Hz, 1 H) 7.27 - 7.35 (m, 4 H) 7.16 - 7.20 (m, 2 H) 7.05 (d, *J*=8.2 Hz, 1 H) 4.65 - 4.72 (m, 1 H) 4.16 - 4.33 (m, 4 H) 3.31 (dd, *J*=13.5, 3.0 Hz, 1 H) 2.78 (dd, *J*=13.2, 9.9 Hz, 1 H) 2.28 (s, 3 H).

(R)-4-Benzyl-3-((R)-2-(4-bromo-2-methylphenyl)propanoyl)oxazolidin-2-one (20)

To a solution of **19** (2.00 g, 5.15 mmol) in THF (20 mL) at -78 °C, was added NaHMDS (1M, THF) (5.67 mL, 5.67 mmol). The pale orange solution was stirred at -78 °C for 65 min, then methyl iodide (1.61 mL, 25.8 mmol) was added. The mixture was stirred at -78 °C for 1.5 h, then was allowed to slowly warm to rt over 4h. The reaction was quenched with sat. NH₄Cl. The mixture was diluted with EtOAc, then washed with H₂O and sat. Na₂SO₃, dried (Na₂SO₄) and concentrated. The crude product was purified by flash chromatography (gradient from 0 to 40 % ethyl acetate/hexanes) to afford **20** (1.35 g, 65 % yield) as a viscous colorless oil. MS (ESI) *m/z* 401.8 (M+H)⁺; ¹H NMR (400 MHz, CDCl₃) δ

1 ppm 7.30 - 7.37 (m, 3 H) 7.22 - 7.29 (m, 4 H) 7.01 (d, $J=8.4$ Hz, 1 H) 5.09 (q, $J=6.9$ Hz, 1 H) 4.62 - 4.67
2 (m, 1 H) 4.06 - 4.15 (m, 2 H) 3.37 (dd, $J=13.4, 3.3$ Hz, 1 H) 2.79 (dd, $J=13.4, 9.9$ Hz, 1 H) 2.39 (s, 3 H)
3
4
5
6
7 1.44 (d, $J=7.0$ Hz, 3 H).
8
9

10 11 12 **(*R*)-2-(4-Bromo-2-methylphenyl)propanoic acid (21)** 13

14
15
16 To a solution of **20** (1.66 g, 4.13 mmol) in THF (20 mL) and water (6.7 mL) at 0 °C, was added a
17
18 solution of lithium peroxide (prepared by adding hydrogen peroxide (1.81 mL, 20.6 mmol) to LiOH
19
20 (0.148 g, 6.19 mmol) in water (7 mL)), dropwise. The mixture was stirred at 0 °C, for 1 h. The reaction
21
22 was quenched with sat. Na₂SO₃ (~10 mL), then the volatiles were removed in vacuo. The mixture was
23
24 diluted with H₂O, then the aqueous solution was extracted with DCM (2X). The aqueous was acidified
25
26 with conc. HCl, then was extracted with EtOAc (2X). The combined organic extracts were washed with
27
28 brine, dried (Na₂SO₄) and concentrated to afford **21** (983 mg, 98 % yield) as a colorless oil. MS (ESI)
29
30 m/z 243.1 (M+H)⁺; ¹H NMR (400 MHz, CDCl₃) δ ppm 7.30 - 7.34 (m, 2 H) 7.16 (d, $J=9.2$ Hz, 1 H) 3.93
31
32 (q, $J=7.0$ Hz, 1 H) 2.35 (s, 3 H) 1.48 (d, $J=7.5$ Hz, 3 H).
33
34
35
36
37
38
39
40
41

42 **(*R*)-2-(4-Bromo-2-methylphenyl)propan-1-ol (22)** 43

44
45 To a solution of **21** (978 mg, 4.02 mmol) in THF (20 mL) at 0 °C, was added Borane-THF (1 M, THF)
46
47 (12.1 mL, 12.1 mmol), dropwise. The mixture was removed from the ice bath and stirred at rt for 65 h.
48
49 The reaction mixture was poured into H₂O (50 mL), then 1N HCl (5 mL) and EtOAc were added. The
50
51 mixture was extracted with EtOAc (2X). The combined organic extract was washed with 0.1 N HCl,
52
53 H₂O and brine, dried (NaSO₄), filtered through a 1" pad of SiO₂ and concentrated to afford **22** (898 mg,
54
55 97 % yield) as a colorless oil. MS (ESI) m/z 211.1 (M - H₂O + H)⁺; ¹H NMR (400 MHz, CDCl₃) δ ppm
56
57
58
59
60

1
2 7.29 - 7.34 (m, 2 H) 7.06 - 7.09 (m, 1 H) 3.65 - 3.75 (m, 2 H) 3.16 - 3.25 (m, 1 H) 2.33 (s, 3 H) 1.32 (t,
3
4 $J=5.9$ Hz, 1 H) 1.22 (d, $J=6.6$ Hz, 3 H).
5
6
7
8
9

10
11 **(*R*)-4-(1-Hydroxypropan-2-yl)-3-methylphenylboronic acid (23)**
12

13
14 To a sealed tube was added **S-7** (500 mg, 2.18 mmol), 5,5,5',5'-tetramethyl-2,2'-bi(1,3,2-dioxaborinane)
15 (592 mg, 2.62 mmol), potassium acetate (535 mg, 5.46 mmol), Pd(dppf)Cl₂ (359 mg, 0.436 mmol) in
16 DMSO (2 mL). The tube was filled with Ar and stirred at 85 °C for 3 h. The mixture was quenched with
17 water, and extracted with EtOAc 3x20 ml. The combined organic layer was filtered through silica gel
18 and concentrated. The product was purified via preparative HPLC to afford **23** (300 mg, 71 % yield) as a
19 colorless solid. MS (ESI) m/z 177.1 (M-OH)⁺; ¹H NMR (400 MHz, CD₃OD) δ 7.35 - 7.61 (m, 2 H),
20 7.16 (d, $J=7.91$ Hz, 1 H), 4.80 (s, 2 H), 3.66 (dd, $J=10.8, 5.9$ Hz, 1 H), 3.52 (dd, $J=10.6, 7.9$ Hz, 1 H),
21 3.15 - 3.21 (m, 1 H), 2.34 (s, 3 H), 1.24 (d, $J=7.03$ Hz, 3 H).
22
23
24
25
26
27
28
29
30
31
32
33
34
35
36

37 ***tert*-Butyl *N*-{6-[(3-aminophenyl)methyl]carbamoyl}{4-[(2*R*)-1-hydroxypropan-2-yl]-3-**
38 **methylphenyl)methyl}amino]isoquinolin-1-yl}-*N*-[(*tert*-butoxy)carbonyl]carbamate (24a)**
39
40

41
42 To a mixture of (*R*)-4-(1-hydroxypropan-2-yl)-3-methylphenylboronic acid (**23**) (64.8 mg, 0.334 mmol),
43 *tert*-butyl *N*-(6-aminoisoquinolin-1-yl)-*N*-[(*tert*-butoxy)carbonyl]carbamate (120 mg, 0.334 mmol), and
44 glyoxylic acid monohydrate (30.7 mg, 0.334 mmol), were added DMF (0.67 mL) and acetonitrile (2
45 mL). The heterogeneous mixture was stirred at 80 °C for 2 h to give an orange solution, which was
46 cooled to rt. To this mixture were added 3-(aminomethyl)aniline (44.9 mg, 0.367 mmol), DMF (2 mL),
47 BOP (162 mg, 0.367 mmol) and TEA (0.233 mL, 1.67 mmol). The mixture was stirred at rt for 1 h. The
48 mixture was partitioned between EtOAc and water. The aqueous phase was extracted with EtOAc. The
49 combined organic phase was washed with H₂O and brine, dried (Na₂SO₄) and concentrated. The crude
50
51
52
53
54
55
56
57
58
59
60

1 product was purified by flash chromatography (1 to 10% methanol/methylene chloride gradient) to
2 afford **24a** (122 mg, 55 % yield) as an off-white solid. MS (ESI) m/z 670.5 (M+H)⁺; ¹H NMR (500MHz,
3 CD₃OD) δ 8.06 (d, $J=5.8$ Hz, 1H), 7.64 (d, $J=9.1$ Hz, 1H), 7.44 (d, $J=5.8$ Hz, 1H), 7.38 - 7.34 (m, 2H),
4
5
6
7
8
9
10
11
12
13
14
15
16
17
18
19
20
21
22
23
24
25
26
27
28
29
30
31
32
33
34
35
36
37
38
39
40
41
42
43
44
45
46
47
48
49
50
51
52
53
54
55
56
57
58
59
60

***tert*-Butyl *N*-{6-[(3-aminophenyl)methyl](methyl)carbonyl}{4-[(2*R*)-1-hydroxypropan-2-yl]-3-methylphenyl}methyl)amino]isoquinolin-1-yl}-*N*-[(*tert*-butoxy)carbonyl]carbamate (**24b**)**

Substituting 3-((methylamino)methyl)aniline for 3-(aminomethyl)aniline afforded **24b** (117 mg, 51 %
yield) as an off-white solid. MS (ESI) m/z 684.5 (M+H)⁺; ¹H NMR (500MHz, CD₃OD) δ 8.03 (dd,
 $J=18.0, 5.9$ Hz, 1H), 7.65 - 7.53 (m, 1H), 7.49 - 7.35 (m, 2H), 7.35 - 7.13 (m, 3H), 7.13 - 6.94 (m, 1H),
6.80 - 6.44 (m, 4H), 5.64 - 5.48 (m, 1H), 4.65 - 4.45 (m, 2H), 3.69 - 3.64 (m, 1H), 3.58 - 3.53 (m, 1H),
3.22 - 3.15 (m, 1H), 3.05 (s, 3H), 2.39 - 2.34 (m, 3H), 1.30 - 1.25 (m, 18H), 1.24 - 1.20 (m, 3H).

(2*S*,15*R*)-2-[(1-Aminoisoquinolin-6-yl)amino]-15,17-dimethyl-13-oxa-4,11-

diazatricyclo[14.2.2.1^{6,10}]henicosa-1(18),6,8,10(21),16,19-hexaene-3,12-dione, TFA salt (26a**)**

(2*R*,15*R*)-2-[(1-Aminoisoquinolin-6-yl)amino]-15,17-dimethyl-13-oxa-4,11-

diazatricyclo[14.2.2.1^{6,10}]henicosa-1(18),6,8,10(21),16,19-hexaene-3,12-dione, TFA salt (27a**)**

To a solution of **24a** (120 mg, 0.179 mmol) in acetonitrile (1.5 mL) and DCM (3 mL) at 0 °C, was added
phosgene (15% in toluene) (0.118 mL, 0.179 mmol), dropwise. The resultant suspension was stirred at 0
°C for 20 min. The suspension was bubbled with Ar for 30 min, then was treated with DMPU (0.1 mL)

1 to give a clear solution. The solution was added dropwise via a syringe pump into a solution of TEA
2 (0.125 mL, 0.896 mmol) in DCM (100 mL) over 3 h. The reaction mixture was stirred at rt for 2 h. The
3
4
5
6
7
8
9
10
11
12
13
14
15
16
17
18
19
20
21
22
23
24
25
26
27
28
29
30
31
32
33
34
35
36
37
38
39
40
41
42
43
44
45
46
47
48
49
50
51
52
53
54
55
56
57
58
59
60

to give a clear solution. The solution was added dropwise via a syringe pump into a solution of TEA (0.125 mL, 0.896 mmol) in DCM (100 mL) over 3 h. The reaction mixture was stirred at rt for 2 h. The reaction mixture was washed with water and brine, dried (Na₂SO₄) and concentrated. The crude product was purified by flash chromatography (0 to 100% ethyl acetate/hexanes gradient) to afford **25a** (51 mg, 41 % yield) as an orange solid. MS (ESI) *m/z* 696.5 (M+H)⁺.

The mixture of diastereomers was separated by chiral prep HPLC (Regis Technologies, Whelk-O1 10/100 FEC 25 cm X 21.1 mm, 80% IPA in heptane, 20 mL/min, RT: 6.04 and 9.06 min). Then, each diastereomer was dissolved in TFA (2 mL), stirred at rt for 30 min, concentrated, and the residue was purified by preparative HPLC.

Macrocycle **26a**: Peak 1. (18.2 mg, 17 % yield from **24a**, 41 % yield from **25a**) white solid. MS (ESI) *m/z* 496.2 (M+H)⁺; HRMS (ESI) *m/z* 496.2342 (-0.32 ppm); ¹H NMR (500MHz, CD₃OD) δ 8.63 (br. s., 1H), 8.07 (d, *J*=9.1 Hz, 1H), 7.45 (d, *J*=1.7 Hz, 1H), 7.34 - 7.32 (m, 1H), 7.31 (d, *J*=1.7 Hz, 1H), 7.29 - 7.24 (m, 1H), 7.21 (dd, *J*=9.2, 2.3 Hz, 1H), 7.14 (t, *J*=7.7 Hz, 1H), 6.90 (dd, *J*=7.7, 0.6 Hz, 1H), 6.87 (d, *J*=7.2 Hz, 1H), 6.72 (d, *J*=1.9 Hz, 1H), 6.69 (dd, *J*=8.0, 1.1 Hz, 1H), 6.18 (s, 1H), 5.13 (s, 1H), 4.81 - 4.74 (m, 1H), 4.63 (dd, *J*=11.0, 3.3 Hz, 1H), 4.19 (dd, *J*=10.7, 5.8 Hz, 1H), 4.05 (dd, *J*=16.1, 4.3 Hz, 1H), 3.50 - 3.42 (m, 1H), 2.48 (s, 3H), 1.38 (d, *J*=6.9 Hz, 3H); Purity: 100 % (method A), 100 % (method B).

Macrocycle **27a**: Peak 2. (16.3 mg, 15 % yield from **24a**, 37 % yield from **25a**) white solid. MS (ESI) *m/z* 496.2 (M+H)⁺; HRMS (ESI) *m/z* 496.2347 (0.79 ppm); ¹H NMR (500MHz, CD₃OD) δ 8.67 (br. s., 1H), 8.06 (d, *J*=9.4 Hz, 1H), 7.52 (dd, *J*=8.0, 1.7 Hz, 1H), 7.43 (d, *J*=8.0 Hz, 1H), 7.31 (d, *J*=7.2 Hz, 1H), 7.25 - 7.17 (m, 2H), 7.14 (t, *J*=7.7 Hz, 1H), 6.90 (dd, *J*=7.7, 0.6 Hz, 1H), 6.86 (d, *J*=6.9 Hz, 1H), 6.72 (d, *J*=1.9 Hz, 1H), 6.67 (dd, *J*=8.0, 1.1 Hz, 1H), 6.11 (s, 1H), 5.16 (s, 1H), 4.77 (dd, *J*=16.4, 7.6 Hz, 1H), 4.65 - 4.54 (m, 1H), 4.21 - 4.13 (m, 1H), 4.07 (dd, *J*=16.5, 4.4 Hz, 1H), 3.55 - 3.41 (m, 1H), 2.34 (s, 3H), 1.32 (d, *J*=6.9 Hz, 3H); Purity: 99.8 % (method A), 96.6 % (method B).

1
2
3
4
5 (2*S*,15*R*)-2-[(1-Aminoisoquinolin-6-yl)amino]-4,15,17-trimethyl-13-oxa-4,11-
6
7 diazatricyclo[14.2.2.1^{6,10}]henicosa-1(18),6,8,10(21),16,19-hexaene-3,12-dione, TFA salt (**26b**)
8
9

10
11 (2*R*,15*R*)-2-[(1-Aminoisoquinolin-6-yl)amino]-4,15,17-trimethyl-13-oxa-4,11-
12
13 diazatricyclo[14.2.2.1^{6,10}]henicosa-1(18),6,8,10(21),16,19-hexaene-3,12-dione, TFA salt (**27b**)
14
15

16 According to the procedure for the cyclization of **24a**, **24b** (115 mg, 0.168 mmol) was cyclized to afford
17
18 **25b** (59 mg, 49 % yield) as an orange solid. MS (ESI) m/z 710.5 (M+H)⁺. The mixture of diastereomers
19
20 was separated by chiral prep HPLC (Regis Technologies, Whelk-O1 10/100 FEC 25 cm X 21.1 mm,
21
22 50% (1:1 MeOH/EtOH) in heptane, 20 mL/min, RT: 6.13 and 9.92 min). Then, each diastereomer was
23
24 dissolved in TFA (2 mL), stirred at rt for 30 min, concentrated, and the residue was purified by
25
26 preparative HPLC.
27
28
29
30

31 Macrocycle **26b**: Peak 1. (23.7 mg, 23 % yield from **24b**, 46% from **25b**) white solid. MS (ESI) m/z
32
33 510.2 (M+H)⁺; HRMS (ESI) m/z 510.2489 (-2.2 ppm); ¹H NMR (500 MHz, CD₃OD) δ 8.05 (d, J=9.35
34
35 Hz, 1H), 7.58 (d, J=1.38 Hz, 1H), 7.31 (t, J=7.84 Hz, 2H), 7.14-7.25 (m, 3H), 6.88-6.95 (m, 2H), 6.84
36
37 (d, J=2.20 Hz, 1H), 6.70 (dd, J=1.10, 7.70 Hz, 1H), 6.04 (s, 1H), 5.72 (s, 1H), 5.43 (d, J=16.23 Hz, 1H),
38
39 4.87-4.94 (m, 1H), 3.84-3.97 (m, 2H), 3.40-3.48 (m, 1H), 3.25 (s, 3H), 2.49 (s, 3H), 1.43 (d, J=7.15 Hz,
40
41 3H); Purity: 99.6 % (method A), 96.6 % (method B).
42
43
44
45

46 Macrocycle **27b**: Peak 2. (19.0 mg, 18 % yield from **24b**, 37% from **25b**) white solid. MS (ESI) m/z
47
48 510.2 (M+H)⁺; HRMS (ESI) m/z 510.2492 (-1.4 ppm); ¹H NMR (500 MHz, CD₃OD) δ 8.05 (d, J=9.35
49
50 Hz, 1H), 7.63 (dd, J=1.79, 7.84 Hz, 1H), 7.43 (d, J=7.98 Hz, 1H), 7.31 (d, J=7.15 Hz, 1H), 7.23 (d,
51
52 J=1.38 Hz, 1H), 7.21 (dd, J=2.48, 9.35 Hz, 1H), 7.18 (t, J=7.84 Hz, 1H), 6.91 (d, J=6.88 Hz, 2H), 6.84
53
54 (d, J=2.20 Hz, 1H), 6.69 (dd, J=0.96, 7.84 Hz, 1H), 5.93 (s, 1H), 5.74 (s, 1H), 5.45 (d, J=16.51 Hz, 1H),
55
56
57
58
59
60

1 4.61-4.69 (m, 1H), 3.96-4.03 (m, 1H), 3.91 (d, J=16.51 Hz, 1H), 3.46-3.55 (m, 1H), 3.29 (s, 3H), 2.34
2 (s, 3H), 1.31 (d, J=6.88 Hz, 3H); Purity: 100 % (method A), 100 % (method B).
3
4
5
6

7 **Crystallization, Data Collection, and Structure Refinement.**

8
9 Procedures followed those described in Priestley et al.⁸ Briefly, recombinant full-length FVIIa was
10 purchased from Novo Nordisk and the GLA domain (residues 1–44) was removed by cathepsin G
11 digestion. Single crystals suitable for X-ray analysis were obtained at 4 °C by hanging drop vapor
12 diffusion with the reservoir containing 20% PEG 6000, 20 mM CaCl₂, 0.1 M MES (pH 6.0). Data for a
13 crystal of the FVIIa/compound **30** complex were collected at 17-ID located at the Advanced Photon
14 Source (APS) using an ADSC Quantum-210 CCD detector. Image data were processed with the
15 program HKL-2000.¹⁹ Refinement was carried out with CNX.²⁰ The structure was re-refined prior to
16 deposition using BUSTER (GlobalPhasing, Ltd., Cambridge, UK), GRADE (GlobalPhasing, Ltd.) for
17 the ligand restraint files, RHOFIT (GlobalPhasing, Ltd.) for ligand placement, and COOT²¹ for electron
18 density map fitting. Coordinates and structure amplitudes for compound **30** have been deposited in the
19 PDB (accession code of 5I46). Compound **3** was previously deposited⁸ with accession code of 4ZXY.
20
21
22
23
24
25
26
27
28
29
30
31
32
33
34
35
36
37
38

39 **Computational Chemistry.**

40
41
42 **Quantum chemical calculations on model systems (Figure 4).** The P2 rotamers were manually built
43 based on previous crystallographic structures of factor VIIa complexed with the phenyl glycine
44 chemotype and molecular modeling.⁸ The aminoisoquinoline was replaced by phenyl to make the
45 calculations more tractable. Geometry optimizations were carried out using B3LYP/ 6-31G** as
46 implemented with defaults in the software program Gaussian.²² Final single point energies were
47 computed at the RI-MP2/cc-pVTZ level of theory using Q-Chem v4.2²³ in the gas phase.
48
49
50
51
52
53
54
55
56
57
58
59
60

1
2 **Conformational search and Boltzmann distribution.** A force field conformational search and
3
4 Boltzmann distribution analysis was conducted using a customized script controlling the software
5
6 program MacroModel, and suggested the bioactive conformation of **7** was highly likely in solution.²⁴
7
8 For the purpose of completeness two sampling methods were utilized in parallel, the Macrocycle
9
10 Sampling²⁵ and mixed Low Mode – Monte Carlo Multiple Minimum (using the LMCS, MCMM
11
12 keywords) algorithms with the OPLS 2.1 forcefield and SGB Born continuum solvent model.²⁶
13
14 Conformations having ≤ 0.6 RMSD Å with respect to atomic coordinates of any other conformation
15
16 after best fit superposition were deemed redundant and removed. Only conformations within 10 kcal of
17
18 the observed global minimum were retained. Conformational free energies were estimated based on the
19
20 rigid – rotor approximation and frequency calculations as implemented in MacroModel, together with
21
22 the forcefield and solvation energies according to the equation:
23
24
25
26

27
28
29 Eq 2. $\epsilon = \text{Gibbs free energy} \approx E_{\text{ff}} + E_{\text{solv}} + H_{\text{vib}} + H_{\text{trans}} + H_{\text{rot}} - (S_{\text{vib}} + S_{\text{trans}} + S_{\text{rot}}) * 298 \text{ K}$
30
31

32 Where
33

34
35 E_{ff} = OPLS 2005 forcefield energy
36

37
38 E_{solv} = Solvation energy from the SGB continuum model
39

40
41 $H_{\text{vib, trans, rot}}$ are the vibrational, rotational, and translational enthalpies
42
43

44
45 $S_{\text{vib, trans, rot}}$ are the vibrational, rotational, and translational entropies
46
47

48 The Boltzmann probability of the j th conformation of N conformations was estimated according to the
49
50 equation:
51
52

53
54 Eq 3.
$$P(\text{Conf}_j) = \frac{e^{-\epsilon_j/kT}}{\sum_i^N e^{-\epsilon_i/kT}}$$

55
56
57
58
59
60

1
2 Where

3
4
5 ε = the conformational free energy estimated from Eq. 2,

6
7
8 $T = 298$ °C,

9
10
11 k = the Boltzmann constant

12
13
14
15 N = the total number of conformations under consideration. Conformations having an excess of 10 kcal
16
17 are neglected.

18
19
20 In equation 3, the numerator is referred to as the Boltzmann weight for the j^{th} conformation and the
21
22 denominator is referred to as the molecular partition function, or the sum of all such weights for all
23
24
25 conformations.
26
27
28
29
30

31 **NMR Experimental**

32
33
34
35
36 **NMR sample preparation.** NMR samples were prepared by dissolution of lyophilized powder of
37
38 macrocyclic FVIIa inhibitors in DMSO- d_6 (CIL-34, D 99.96%) in the concentration range of 3 – 7 mM
39
40 and placed in a 5 mm NMR tube.
41
42
43
44

45
46 **NMR data acquisition of unsubstituted macrocycle 3.** A sample of **3** was prepared at 3.0 mM in
47
48 DMSO- d_6 . The following NMR spectra were recorded on a Varian Inova 600 MHz spectrometer which
49
50 was equipped with a Cold probe: a) experiments at 25 °C; HC-HSQC, HC-HMBC, PECOSY, NOESY
51
52 ($\tau_m = 150$ ms & 300 ms), TOCSY ($\tau_m = 70$ ms), b) chemical exchange experiments; NOESY ($\tau_m = 1000$
53
54 ms) recorded at 22, 26.5, 31.0, 35.5, 41.0, 44.5, 49.0 °C. The spectra were manually assigned in *Felix*
55
56 using the ACD/NMR²⁷-predicted chemical shifts as starting points and entered into a *Felix* database.
57
58
59
60

1
2 The HC-HMQC spectrum featured a large number of 3-bond HC-couplings which facilitated the
3
4 confirmation of resonance assignments.
5

6
7 Additional spectral parameters:
8

9
10 TOCSY, NOESY spectra: sw1 = sw = 900 Hz, number of complex t₁-data points = 512, acquisition time
11
12 = 0.3 sec, number of scan per t₁-point = 8 (TOCSY), 32 (NOESY), States-Haberkm acquisition
13
14 mode²⁸, relaxation delay = 2.5 sec (TOCSY), 3.0 sec (NOESY).
15

16
17 HC-HMQC spectra: Sw1 = 10543 Hz, sw = 9000 Hz, number of complex t₁-data points = 256,
18
19 acquisition time = 0.15 sec, number of scans per t₁-point = 48, States-Haberkm acquisition mode,
20
21 relaxation delay = 2.5 sec, long-range J-coupling delay = 0.062 sec (corresponding to a long-range J-
22
23 coupling of ~ 8 Hz).
24

25
26 **Evaluating time-dependence of phenyl ring flips in macrocycle 3.** Chemical exchange rates were
27
28 calculated from the ratios of diagonal and cross peaks between phenyl protons H17 & H21 using the
29
30 equation $k_{ex} = (V_{h17,h21}) / (V_{h17,h17} + V_{h17,h21}) * (1/\tau_m)$.²⁹ The ln(k_{ex}) was subjected to a linear regression fit
31
32 against 1/T in MS Excel using the Trendline fitting protocol [$\ln(k_{ex}) = \ln(A) - (E_a/R) * (1/T)$, where T =
33
34 absolute temperature]. This produced the following fit: $\ln(A) = 17.2$, $E_a = 12.4$ kcal/mole, $R^2 = 0.992$.
35
36 These values set the lifetime of the phenyl ring rotamer state in the macrocycle to ~ 3 sec at 70 °C and ~
37
38 67 sec at 20 °C.
39
40
41
42

43
44 **NMR-resonance assignments.** Proton and carbon-13 resonances were assigned manually starting from
45
46 ACD/NMR²⁷ predicted proton and carbon chemical shifts. NOE-distance restraints were generated in
47
48 nmrView (version 9.1.0-b17, Onemoon Scientific, Inc.) from cross-peak elliptical volumes in the
49
50 NOESY spectra, which were acquired at a mixing time of 0.3 sec. The lower bounds were set to 1.8 Å,
51
52 and the upper bounds were set to the estimated square of the respective inter-proton distances multiplied
53
54 by the scaling factor 0.125. The cross-peak volumes were translated to inter-proton distances using
55
56 volumes of well-resolved cross-peaks of vicinal aromatic proton pairs.
57
58
59
60

1 **XPLOR-structure calculations of macrocycle 3.** XPLOR-files of compound **3** were generated in
2
3
4 Quanta (Accelrys, Inc.) starting from a CHARMM-minimized structural model. To ensure planarity of
5
6 aromatic rings and peptide bonds, torsion-angle restraints were introduced. In addition, the
7
8 configurations of chiral- and pro-chiral carbons were preserved by improper angle restraints. Two sets of
9
10 structures were generated using a simulated annealing script utilizing a model structure with NOE-
11
12 distance restraints which were compatible with chair- and saddle conformer in the hydrocarbon linker
13
14 respectively. The seed defining initial velocity vectors randomly varied between successive structure-
15
16 anneal runs. Two torsion angle restraints derived from J_{HN,Ha}-coupling constants were employed. The
17
18 NOE-distance restraints were generated in nmrView from cross-peak volumes in the NOESY spectrum,
19
20 which was acquired with a mixing period of 0.3 sec. Both cross peaks between the most resolved
21
22 resonances of vicinal aromatic proton pairs were employed, i.e., the cross peaks between H30 & H29.
23
24 With a couple of exceptions, the default lower bounds were set to 1.8 Å. The upper bounds of the
25
26 distance restraints were set using the default protocol in nmrView, i.e., the upper bounds were set to the
27
28 square of cross-peak volume-based inter-proton distances times the scaling factor of 0.125.
29
30
31
32
33

34
35 The average structure was calculated from converged structures that feature no NOE-violations in
36
37 excess of 0.15 Å. The converged XPLOR-structures were superimposed with the average structures
38
39 using non-hydrogen atoms in the macrocycle excluding carbonyl oxygen atoms in Maestro. The average
40
41 rmsd of macrocycle heavy atoms to the average structure was 0.24 Å and 0.21 Å in the saddle and the
42
43 chair conformers, respectively.
44
45
46
47
48
49

50 **NOE-difference experiments of methyl-substituted, carbamate-linked macrocycle 5.** NOE-
51
52 difference spectra³⁰ were recorded in a 6.2 mM sample of compound **5** on a Bruker Avance III 700 MHz
53
54 spectrometer, which was equipped with a 5 mm TCI cryogenic probe. A slightly modified version of the
55
56 Bruker “noediffgp”-pulse program was employed, which was augmented with the purging pulse pair of
57
58
59
60

12.5 kHz amplitude and durations of 2.5 msec and 3.52 msec respectively at the start of the relaxation delay (See Supplemental section). In addition, a composite proton 180° pulse was inserted in alternate scans while the phase of the receiver was inverted. This had the effect of suppressing signal that was created by longitudinal T₁-relaxation during the CW-irradiation period. A total of three spectra were acquired concurrently, one with the 2 Hz amplitude CW-irradiation field set off-resonance by 2000 Hz, one with the CW-irradiation set to the resonance frequency of methyl peak 1, and one with the CW-irradiation field set to the resonance frequency of methyl resonance 2. Difference spectra were calculated by subtracting spectra 2 and 3 from the off-resonance irradiation spectrum 1. Four-fold block-averaging was employed, resulting in a total number of 32 scans per fid. The relaxation delay was set to 4 sec, and the acquisition period to 1 sec. The sample temperature was increased in 10 °C steps from 20 °C to 70 °C. The duration of the selective irradiation interval was set to 1.0 sec.

Eq. 4 $k_{\text{ex}} = \text{average}(i=1,2) \{ (1 / \tau^{\text{m}}) * I_{\text{corr}}^{\text{cross}}_i / (I_{\text{irrad}}_i + I_{\text{corr}}^{\text{cross}}_i),$

where τ^{m} is the CW-irradiation period, and I_{irrad} and $I_{\text{corr}}^{\text{cross}}$ are the intensities of the irradiated methyl peak,

$I_{\text{corr}}^{\text{cross}}_i = I_{\text{cross}}_i - I_{\text{dia}}^{\text{dia}} * [\omega_1 / (\sigma_i - \sigma_j)]^2$ and the chemical exchange-induced methyl peak. The cross-peak

correction factor accounts for the effect of low power irradiation field on the cross peak intensity.

Averaged chemical exchange rates k_{ex} were calculated using Eq. 4, which represents a modified version of the equation of two-site exchange phenomenon in NOESY spectra.²⁹ Averaging was done to improve accuracy and to correct for the slight imbalance in population of the two observed conformers. The aim of the small correction factors applied to the cross-peak intensities in Eq. 4 was to eliminate the effect of direct saturation of methyl resonance 2 while irradiating methyl 1 or vice versa. Fitting of the $\ln(k_{\text{ex}})$ -values to $1/T$ was performed in MS Excel using its Trendline function (see Supporting Information).

1 **NMR data acquisition in carbamate-linked macrocycle 27a.** Proton 1d spectra and the following
2 suite of 2D NMR spectra were acquired in a sample of 6 mM in DMSO-d₆ in a 5 mm tube on a Bruker
3 AvanceIII 700 MHz spectrometer which was equipped with a 5 mm TCI cryogenic probe. List of 2D
4 NMR experiments: magnitude COSY,³¹ PECOSY,³² TOCSY,^{33,34} NOESY,^{35,36} DEPT-edited HC-
5 HSQC,³⁷ HC-HMBC.³⁸
6
7 Spectral widths in proton 2D experiments: 14 & 12 ppm in F₂ and F₁ respectively, with the exception of
8 the PECOSY where sw1 = 14 ppm. The number of data acquisition points in t₂ & t₁ in the proton 2D
9 experiments were set to 4096 & 1280 except for the magnitude COSY, where the number of t₁-points
10 was set to 2048, and the PECOSY, where the number of t₁-points was set to 4096. At least two-fold zero
11 filling was employed during data processing. In the proton 2D-spectra, a cosine square apodization
12 function was employed in all time domains. In the magnitude COSY spectra a sine bell apodization
13 function was employed in both time domains and in the PECOSY spectra a 45 degree shifted sine bell
14 function was employed in both time domains. TOCSY-spectra: A modified version of the Bruker library
15 pulse program “mlevphpp” was employed, where a purging pulse pair was employed at the start of the
16 relaxation delay, the TOCSY mixing period was set to 0.07 sec and the amplitude of the TOCSY
17 irradiation field was set to 10.4 kHz, the relaxation delay was set to 2.7 sec, the number of scans per t₁-
18 point was set to 2. Magnitude COSY: ns = 1, relaxation delay = 2.7 sec. NOESY: A modified version of
19 the phase-sensitive NOESY pulse program in the Bruker program library was employed. Implemented
20 modifications: Purging pulse pair at the start of the relaxation delay, block-averaging of data acquisition,
21 where an entire 2D-time domain interferogram was acquired with ns = 2, followed by super-positions of
22 additional time domain interferograms with the total number of scans per t₁-point being 2 * 3 (co-
23 addition of 3 time domain interferograms). Implementation of block-averaging was performed by
24 Wolfgang Bermel, Bruker-Biospin. 2D NMR spectra, which are acquired by block-averaging, feature
25 reduced t₁-noise on AvanceIII spectrometers (in-house tests, unpublished).
26
27
28
29
30
31
32
33
34
35
36
37
38
39
40
41
42
43
44
45
46
47
48
49
50
51
52
53
54
55
56
57
58
59
60

1 DEPT-edited HSQC spectra³⁷ were acquired with sign-inversion of cross peaks in CH₂-groups. The
2 DEPT-HSQC spectra were processed with cosine-squared apodization in both t₁ and t₂. The spectra were
3 phased such that CH- and CH₃ groups produced positive cross peaks and CH₂-groups produced negative
4 cross peaks. The HC-HMBC³⁸ spectra were acquired with the long-range coupling delay being set to
5 maximize transfer at a long-range J-coupling of 9 Hz. The t₁-domain interferograms were reconstructed
6 for echo- and anti-coherence transfer echoes. Data processing in F₁ was done in the phase-sensitive
7 mode in F1 and magnitude mode in F2. A cosine square apodization function was applied in t₁. In t₂ a
8 sine apodization function was applied, and the magnitude spectrum was calculated along the F₂-proton
9 dimension. All spectra processing was done in topspin 3.2 (Bruker BioSpin, Inc.). Processed spectra
10 were imported into nmrView (version 9.1.0-b17, Onemoon Scientific, Inc. Westfield, NJ USA) for
11 resonance assignments and the generation of XPLOR-type distance restraints.
12
13
14
15
16
17
18
19
20
21
22
23
24
25
26
27

28 **XPLOR structure calculations in compound 27a.** An initial model of the structure of compound **27a**
29 was built in Maestro (V10.2.010, Schrodinger, Inc.). Fractional charges and energy minimizations to
30 optimize local geometries were performed using the force field OPLS2.1 with implicit water. The
31 energy-minimized structure was exported in mol2-format. This mol2-structure served as input to the
32 Python script “acpype”³⁹ (gift from E. D. Laue, University of Cambridge). The acpype script was
33 instructed to preserve the Maestro-generated fractional charges during the calculation of the CNS-type
34 parameter and topology file. The acpype script also created a randomized pdb-format structure, as well
35 an XPLOR-input, which subsequently was executed to produce the XPLOR-compatible psf-file. In our
36 laboratory, acpype has proven to be a valuable tool for generating XPLOR parameter and psf-files for
37 organic compounds. Acpype produced some entries in the parameter file which yielded high energy
38 structures. These restraints were iteratively eliminated by computing energy-minimized structures in
39 XPLOR-amended CNS parameter files. As in the XPLOR-calculations of the structure in compound 3,
40 aromatic rings and peptide bonds were kept planar by the introduction of torsion-angle restraints.
41
42
43
44
45
46
47
48
49
50
51
52
53
54
55
56
57
58
59
60

1 Configurations of chiral and pro-chiral carbons were preserved by “improper” torsion angle
2 restraints. Acypype also produced a randomized pdb structure, which was used as the initial conformation
3
4 in the XPLOR-structure calculations. Structure calculations were performed using a simulated annealing
5
6 script in XPLOR-nih Linux version 2.37. Average structures and analysis of distance violations were
7
8 performed using XPLOR-scripts.
9

10
11
12 NOE-distance restraints were generated from elliptic cross peak volumes in nmrView. The cross-peak
13
14 volumes were calibrated using the well-resolved cross-peak pairs between the proton resonances of
15
16 (H30, H60) & (H10 & H50). A total of 28 NOE-derived distance restraints were employed, which were
17
18 generated in nmrView cross cross peak volumes as described in the experimental section depicting
19
20 XPLOR-calculations in compound **3**. Fifteen out of 20 annealed structures converged with no distance
21
22 violation in excess of 0.15 Å. An average structure was calculated of the ensemble of converged
23
24 structures using a pertinent XPLOR-input script. The average rmsd of non-hydrogen atoms of the
25
26 converged structures to the average structure was 0.075 Å. A superposition of the ensemble of
27
28 converged NMR structures to the FVIIa bound crystal structure of an analogous compounds exhibited a
29
30 high degree of similarity.
31
32
33
34
35
36
37

38 **Biological Assays.** The TF/FVIIa, FXa, FXIa, thrombin, trypsin, and tissue kallikrein 1 enzyme assays
39
40 were performed according to published protocols.¹⁷
41
42
43
44

45 **ACKNOWLEDGMENT.** We thank Jeffrey Bozarth, Mojgan Abousleiman, and Randi Brown for
46
47 conducting biological assays. We thank Robert Langish for generating high-resolution mass
48
49 spectrometry data. We thank colleagues at the BMS-Biocon Research Center for synthesis of *tert*-butyl
50
51 *N*-(6-aminoisoquinolin-1-yl)-*N*-[(*tert*-butoxy)carbonyl]carbamate. Use of the IMCA-CAT beamline 17-
52
53 BM at the Advanced Photon Source was supported by the companies of the Industrial Macromolecular
54
55 Crystallography Association through a contract with the Center for Advanced Radiation Sources at the
56
57
58
59
60

1 University of Chicago. Use of the Advanced Photon Source was supported by the U.S. Department of
2 Energy, Office of Science, Office of Basic Energy Sciences, under Contract No. DE-AC02-06CH11357.
3

4 We thank Steven Sheriff both for preparing the coordinates and data of compound **30** complexed to
5 factor VIIa and depositing them in the PDB. The authors would also like to thank John Shelley and
6 Shawn Watts, both of Schrodinger, Inc., for developing the automated procedure for the thermodynamic
7 conformational analysis described in this paper. We also thank Wolfgang Bermel at Bruker-Biospin for
8 encoding the NOESY-pulse program which incorporated block-averaged acquisition of the t_1 -
9 interferograms. Ernest Laue at Cambridge University is thanked for providing us with the “acpye”-
10 Python script for the generation of CNS-parameter and topology files.
11
12
13
14
15
16
17
18
19
20
21
22
23
24
25
26

27 AUTHOR INFORMATION

28
29
30 * To whom correspondence should be addressed. Phone: (609) 466-5041. Fax: (609) 818-3331. E-mail:

31
32 peter.glunz@bms.com.
33
34
35
36
37
38

39 ABBREVIATIONS USED

40
41
42 TF/FVIIa, tissue factor/factor VIIa; Fxa, factor Xa; FXIa, factor XIa; Tissue kall, tissue kallikrein 1;
43 Phg, phenylglycine; RMSD, root-mean-square deviation; PyBOP, (benzotriazol-1-
44 yloxy)tripyrrolidinophosphonium hexafluorophosphate; PECOSY, primitive exclusive correlated
45 spectroscopy; TOCSY, total correlation spectroscopy; HC-HSQC, hydrogen-carbon heteronuclear single
46 quantum correlation; HC-HMBC, hydrogen-carbon heteronuclear multiple bond correlation
47
48
49
50
51
52
53
54
55
56
57

58 **SUPPORTING INFORMATION AVAILABLE:**
59
60

1
2 Synthesis of compounds **6**, **28**, **29** and **30**, Boltzmann distribution of conformers of macrocycle **7**,
3
4 additional NMR experiments and data for compounds **3**, **5** and **27a**
5
6

7 Molecular formula strings (CSV)
8
9
10
11
12

13 REFERENCES

- 14
15
16
17 (1) Ōki, M. Recent advances in atropisomerism. In *Topics in Stereochemistry*, John Wiley & Sons,
18 Inc.: Hoboken, NJ, 2007; pp 1-81.
19
20
21 (2) Bringmann, G.; Price Mortimer, A. J.; Keller, P. A.; Gresser, M. J.; Garner, J.; Breuning, M.
22 Atroposelective synthesis of axially chiral biaryl compounds. *Angew. Chem., Int. Ed.* **2005**, *44*, 5384-
23 5427.
24
25
26
27
28 (3) (a) Singh, S. B.; Jayasuriya, H.; Salituro, G. M.; Zink, D. L.; Shafiee, A.; Heimbuch, B.; Silverman,
29 K. C.; Lingham, R. B.; Genilloud, O.; Teran, A.; Vilella, D.; Felock, P.; Hazuda, D. The Complestatins
30 as HIV-1 integrase inhibitors. Efficient isolation, structure elucidation, and inhibitory activities of
31 isocomplestatin, chloropectin I, new complestatins, A and B, and acid-hydrolysis products of
32 chloropectin I. *J. Nat. Prod.* **2001**, *64*, 874-882; (b) Shimamura, H.; Breazzano, S. P.; Garfunkle, J.;
33 Kimball, F. S.; Trzupek, J. D.; Boger, D. L. Total synthesis of complestatin: Development of a Pd(0)-
34 mediated indole annulation for macrocyclization. *J. Am. Chem. Soc.* **2010**, *132*, 7776-7783.
35
36
37
38 (4) (a) Schäfer, M.; Schneider, T. R.; Sheldrick, G. M. Crystal structure of vancomycin. *Structure*
39 **1996**, *4*, 1509-1515; (b) Boger, D. L.; Loiseleur, O.; Castle, S. L.; Beresis, R. T.; Wu, J. H. Thermal
40 atropisomerism of fully functionalized vancomycin CD, DE, and CDE ring systems. *Bioorg. Med.*
41 *Chem. Lett.* **1997**, *7*, 3199-3202.
42
43
44
45 (5) LaPlante, S. R.; Edwards, P. J.; Fader, L. D.; Jakalian, A.; Hucke, O. Revealing atropisomer axial
46
47
48
49
50
51
52
53
54
55
56
57
58
59
60

1
2 (6) Clayden, J.; Moran, W. J.; Edwards, P. J.; LaPlante, S. R. The challenge of atropisomerism in drug
3
4 discovery. *Angew. Chem., Int. Ed.* **2009**, *48*, 6398-6401.

5
6 (7) (a) Driggers, E. M.; Hale, S. P.; Lee, J.; Terrett, N. K. The exploration of macrocycles for drug
7
8 discovery-an underexploited structural class. *Nat. Rev. Drug Discovery* **2008**, *7*, 608-624; (b)

9
10
11 Mallinson, J.; Collins, I. Macrocycles in new drug discovery. *Future Med. Chem.* **2012**, *4*, 1409-1438.

12
13 (8) Priestley, E. S.; Cheney, D. L.; DeLucca, I.; Wei, A.; Luetzgen, J. M.; Rendina, A. R.; Wong, P. C.;
14
15 Wexler, R. R. Structure-based design of macrocyclic coagulation Factor VIIa inhibitors. *J. Med. Chem.*
16
17 **2015**, *58*, 6225-6236.

18
19 (9) (a) Kadono, S.; Sakamoto, A.; Kikuchi, Y.; Oh-eda, M.; Yabuta, N.; Koga, T.; Hattori, K.;
20
21 Shiraishi, T.; Haramura, M.; Kodama, H.; Esaki, T.; Sato, H.; Watanabe, Y.; Itoh, S.; Ohta, M.; Kozono,
22
23 T. Peptide mimetic factor VIIa inhibitor: Importance of hydrophilic pocket in S2 site to improve
24
25 selectivity against thrombin. *Lett. Drug Des. Discovery* **2005**, *2*, 177-181; (b) Krishnan, R.; Kotian, P.
26
27 L.; Chand, P.; Bantia, S.; Rowland, S.; Babu, Y. S. Probing the S2 site of factor VIIa to generate potent
28
29 and selective inhibitors: the structure of BCX-3607 in complex with tissue factor-factor VIIa. *Acta*
30
31 *Crystallogr., Sect. D: Biol. Crystallogr.* **2007**, *63*, 689-697.

32
33 (10) Normalized cross peak intensity was fitted to an Arrhenius equation to arrive at this energy.

34
35 (11) Glunz, P. W.; Cheng, X.; Cheney, D. L.; Weigelt, C. A.; Wei, A.; Luetzgen, J. M.; Wong, P. C.;
36
37 Wexler, R. R.; Priestley, E. S. Design and synthesis of potent, selective phenylimidazole-based FVIIa
38
39 inhibitors. *Bioorg. Med. Chem. Lett.* **2015**, *25*, 2169-2173.

40
41 (12) (a) Petasis, N. A.; Zavialov, I. A. A new and practical synthesis of α -amino acids from alkenyl
42
43 boronic acids. *J. Am. Chem. Soc.* **1997**, *119*, 445-446; (b) Candeias, N. R.; Montalbano, F.; Cal, P. M.
44
45 S. D.; Gois, P. M. P. Boronic acids and esters in the Petasis-borono Mannich multicomponent reaction.
46
47 *Chem. Rev.* **2010**, *110*, 6169-6193.
48
49
50
51
52
53
54
55
56
57
58
59
60

- 1
2 (13) Glunz, P. W.; Bisacchi, G. S.; Morton, G. C.; Holubec, A. A.; Priestley, E. S.; Zhang, X.; Treuner,
3
4 U. D. Preparation of phenylglycine sulfonamide derivatives useful as serine protease inhibitors.
5
6 WO2004072101A2, 2004.
7
8
9 (14) Borgono, C. A.; Diamandis, E. P. The emerging roles of human tissue kallikreins in cancer. *Nat.*
10
11 *Rev. Cancer* **2004**, *4*, 876-890.
12
13 (15) Prassas, I.; Eissa, A.; Poda, G.; Diamandis, E. P. Unleashing the therapeutic potential of human
14
15 kallikrein-related serine proteases. *Nat. Rev. Drug Discovery* **2015**, *14*, 183-202.
16
17
18 (16) Zhang, X.; Glunz, P. W.; Johnson, J. A.; Jiang, W.; Jacutin-Porte, S.; Ladziata, V.; Phillips, M. S.;
19
20 Wurtz, N. R.; Parkhurst, B.; Rendina, A. R.; Harper, T. M.; Cheney, D. L.; Luetzgen, J. M.; Wong, P. C.;
21
22 Seiffert, D.; Wexler, R. R.; Priestley, E. S. Discovery of a highly potent, selective, and orally
23
24 bioavailable macrocyclic inhibitor of blood coagulation factor VIIa-tissue factor complex. *in*
25
26 *preparation*.
27
28
29 (17) Wong, P. C.; Luetzgen, J. M.; Rendina, A. R.; Kettner, C. A.; Xin, B.; Knabb, R. M.; Wexler, R.;
30
31 Priestley, E. S. BMS-593214, an active site-directed factor VIIa inhibitor: Enzyme kinetics,
32
33 antithrombotic and antihaemostatic studies. *Thromb. Haemostasis* **2010**, *104*, 261-269.
34
35
36 (18) *The PyMOL Molecular Graphics System*, Version 1.7 Schrödinger, LLC.
37
38
39 (19) Otwinowski, Z.; Minor, W. Processing of X-ray diffraction data collected in oscillation mode.
40
41 *Methods Enzymol.* **1997**, *276*, 307-326.
42
43
44 (20) Brünger, A. T.; Adams, P. D.; Clore, G. M.; DeLano, W. L.; Gros, P.; Grosse-Kunstleve, R. W.;
45
46 Jiang, J.-S.; Kuszewski, J.; Nilges, M.; Pannu, N. S. Crystallography & NMR system: A new software
47
48 suite for macromolecular structure determination. *Acta Crystallogr., Sect. D: Biol. Crystallogr.* **1998**,
49
50 *54*, 905-921.
51
52
53 (21) Emsley, P.; Lohkamp, B.; Scott, W. G.; Cowtan, K. Features and development of Coot. *Acta*
54
55 *Crystallogr., Sect. D: Biol. Crystallogr.* **2010**, *66*, 486-501.
56
57
58
59
60

1
2 (22) Frisch, M. J.; Trucks, G. W.; Schlegel, H. B.; Scuseria, G. E.; Robb, M. A.; Cheeseman, J. R.;
3
4 Scalmani, G.; Barone, V.; Mennucci, B.; Petersson, G. A.; Nakatsuji, H.; Caricato, M.; Li, X.;
5
6 Hratchian, H. P.; Izmaylov, A. F.; Bloino, J.; Zheng, G.; Sonnenberg, J. L.; Hada, M.; Ehara, M.;
7
8 Toyota, K.; Fukuda, R.; Hasegawa, J.; Ishida, M.; Nakajima, T.; Honda, Y.; Kitao, O.; Nakai, H.;
9
10 Vreven, T.; Montgomery Jr., J. A.; Peralta, J. E.; Ogliaro, F.; Bearpark, M. J.; Heyd, J.; Brothers, E. N.;
11
12 Kudin, K. N.; Staroverov, V. N.; Kobayashi, R.; Normand, J.; Raghavachari, K.; Rendell, A. P.; Burant,
13
14 J. C.; Iyengar, S. S.; Tomasi, J.; Cossi, M.; Rega, N.; Millam, N. J.; Klene, M.; Knox, J. E.; Cross, J. B.;
15
16 Bakken, V.; Adamo, C.; Jaramillo, J.; Gomperts, R.; Stratmann, R. E.; Yazyev, O.; Austin, A. J.;
17
18 Cammi, R.; Pomelli, C.; Ochterski, J. W.; Martin, R. L.; Morokuma, K.; Zakrzewski, V. G.; Voth, G.
19
20 A.; Salvador, P.; Dannenberg, J. J.; Dapprich, S.; Daniels, A. D.; Farkas, Ö.; Foresman, J. B.; Ortiz, J.
21
22 V.; Cioslowski, J.; Fox, D. J. *Gaussian 09*, Gaussian, Inc.: Wallingford, CT, USA, 2009.

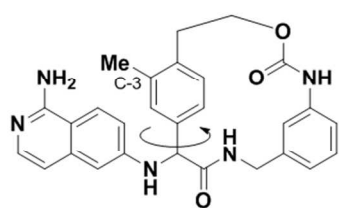
23
24
25
26
27 (23) Shao, Y.; Gan, Z.; Epifanovsky, E.; Gilbert, A. T. B.; Wormit, M.; Kussmann, J.; Lange, A. W.;
28
29 Behn, A.; Deng, J.; Feng, X.; Ghosh, D.; Goldey, M.; Horn, P. R.; Jacobson, L. D.; Kaliman, I.;
30
31 Khaliullin, R. Z.; Kuś, T.; Landau, A.; Liu, J.; Proynov, E. I.; Rhee, Y. M.; Richard, R. M.; Rohrdanz,
32
33 M. A.; Steele, R. P.; Sundstrom, E. J.; Woodcock, H. L.; Zimmerman, P. M.; Zuev, D.; Albrecht, B.;
34
35 Alguire, E.; Austin, B.; Beran, G. J. O.; Bernard, Y. A.; Berquist, E.; Brandhorst, K.; Bravaya, K. B.;
36
37 Brown, S. T.; Casanova, D.; Chang, C.-M.; Chen, Y.; Chien, S. H.; Closser, K. D.; Crittenden, D. L.;
38
39 Diedenhofen, M.; DiStasio, R. A.; Do, H.; Dutoi, A. D.; Edgar, R. G.; Fatehi, S.; Fusti-Molnar, L.;
40
41 Ghysels, A.; Golubeva-Zadorozhnaya, A.; Gomes, J.; Hanson-Heine, M. W. D.; Harbach, P. H. P.;
42
43 Hauser, A. W.; Hohenstein, E. G.; Holden, Z. C.; Jagau, T.-C.; Ji, H.; Kaduk, B.; Khistyayev, K.; Kim, J.;
44
45 Kim, J.; King, R. A.; Klunzinger, P.; Kosenkov, D.; Kowalczyk, T.; Krauter, C. M.; Lao, K. U.; Laurent,
46
47 A. D.; Lawler, K. V.; Levchenko, S. V.; Lin, C. Y.; Liu, F.; Livshits, E.; Lochan, R. C.; Luenser, A.;
48
49 Manohar, P.; Manzer, S. F.; Mao, S.-P.; Mardirossian, N.; Marenich, A. V.; Maurer, S. A.; Mayhall, N.
50
51 J.; Neuscammann, E.; Oana, C. M.; Olivares-Amaya, R.; O'Neill, D. P.; Parkhill, J. A.; Perrine, T. M.;
52
53 Peverati, R.; Prociuk, A.; Rehn, D. R.; Rosta, E.; Russ, N. J.; Sharada, S. M.; Sharma, S.; Small, D. W.;
54
55
56
57
58
59
60

- 1 Sodt, A.; Stein, T.; Stück, D.; Su, Y.-C.; Thom, A. J. W.; Tsuchimochi, T.; Vanovschi, V.; Vogt, L.;
2
3
4 Vydrov, O.; Wang, T.; Watson, M. A.; Wenzel, J.; White, A.; Williams, C. F.; Yang, J.; Yeganeh, S.;
5
6
7 Yost, S. R.; You, Z.-Q.; Zhang, I. Y.; Zhang, X.; Zhao, Y.; Brooks, B. R.; Chan, G. K. L.; Chipman, D.
8
9 M.; Cramer, C. J.; Goddard, W. A.; Gordon, M. S.; Hehre, W. J.; Klamt, A.; Schaefer, H. F.; Schmidt,
10
11 M. W.; Sherrill, C. D.; Truhlar, D. G.; Warshel, A.; Xu, X.; Aspuru-Guzik, A.; Baer, R.; Bell, A. T.;
12
13 Besley, N. A.; Chai, J.-D.; Dreuw, A.; Dunietz, B. D.; Furlani, T. R.; Gwaltney, S. R.; Hsu, C.-P.; Jung,
14
15 Y.; Kong, J.; Lambrecht, D. S.; Liang, W.; Ochsenfeld, C.; Rassolov, V. A.; Slipchenko, L. V.;
16
17 Subotnik, J. E.; Van Voorhis, T.; Herbert, J. M.; Krylov, A. I.; Gill, P. M. W.; Head-Gordon, M.
18
19
20 Advances in molecular quantum chemistry contained in the Q-Chem 4 program package. *Mol. Phys.*
21
22 **2014**, *113*, 184-215.
23
24
25 (24) Glunz, P. W.; Zhang, X.; Zou, Y.; Delucca, I.; Nirschl, A. H.; Cheng, X.; Weigelt, C. A.; Cheney,
26
27 D. L.; Wei, A.; Anumula, R.; Luetzgen, J. M.; Rendina, A. R.; Harpel, M.; Luo, G.; Knabb, R.; Wong, P.
28
29 C.; Wexler, R. R.; Priestley, E. S. Nonbenzamidine acylsulfonamide tissue factor-factor VIIa inhibitors.
30
31 *Bioorg. Med. Chem. Lett.* **2013**, *23*, 5244-5248.
32
33
34 (25) Watts, K. S.; Dalal, P.; Tebben, A. J.; Cheney, D. L.; Shelley, J. C. Macrocyclic conformational
35
36 sampling with MacroModel. *J. Chem. Inf. Model.* **2014**, *54*, 2680-2696.
37
38
39 (26) Priestley, E. S.; De Lucca, I.; Zhou, J.; Zhou, J.; Saiah, E.; Stanton, R.; Robinson, L.; Luetzgen, J.
40
41 M.; Wei, A.; Wen, X.; Knabb, R. M.; Wong, P. C.; Wexler, R. R. Discovery and gram-scale synthesis of
42
43 BMS-593214, a potent, selective FVIIa inhibitor. *Bioorg. Med. Chem. Lett.* **2013**, *23*, 2432-2435.
44
45
46 (27) *ACD/NMR*, v. 10, Advanced Chemistry Development, Inc., Toronto, ON, Canada,
47
48 www.acdlabs.com, 2006.
49
50
51 (28) States, D. J.; Haberkorn, R. A.; Ruben, D. J. A two-dimensional nuclear Overhauser experiment
52
53 with pure absorption phase in four quadrants. *J. Magn. Reson.* **1982**, *48*, 286-292.
54
55
56 (29) Ernst, R. R.; Bodenhausen, G.; Wokaun, A. *Principles of Nuclear Magnetic Resonance in One*
57
58 *and Two Dimensions*. Clarendon Press: Oxford, 1987; Vol. 14.
59
60

- 1
2 (30) Neuhaus, D.; Sheppard, R. N.; Bick, I. R. C. Structural and conformational study of repanduline
3 using long-range nuclear Overhauser effect difference spectroscopy. *J. Am. Chem. Soc.* **1983**, *105*, 5996-
4 6002.
5
6
7
8 (31) Aue, W. P.; Bartholdi, E.; Ernst, R. R. Two-dimensional spectroscopy. Application to nuclear
9 magnetic resonance. *J. Chem. Phys.* **1976**, *64*, 2229-2246.
10
11 (32) Mueller, L. P.E.COSY, a simple alternative to E.COSY. *J. Magn. Reson.* **1987**, *72*, 191-6.
12
13 (33) Bax, A.; Davis, D. G. MLEV-17-based two-dimensional homonuclear magnetization transfer
14 spectroscopy. *J. Magn. Reson.* **1985**, *65*, 355-360.
15
16 (34) Braunschweiler, L.; Ernst, R. R. Coherence transfer by isotropic mixing: application to proton
17 correlation spectroscopy. *J. Magn. Reson.* **1983**, *53*, 521-528.
18
19 (35) Jeener, J.; Meier, B. H.; Bachmann, P.; Ernst, R. R. Investigation of exchange processes by two-
20 dimensional NMR spectroscopy. *J. Chem. Phys.* **1979**, *71*, 4546-4553.
21
22 (36) Kumar, A.; Ernst, R. R.; Wuthrich, K. A two-dimensional nuclear Overhauser enhancement (2D
23 NOE) experiment for the elucidation of complete proton-proton cross-relaxation networks in biological
24 macromolecules. *Biochem. Biophys. Res. Commun.* **1980**, *95*, 1-6.
25
26 (37) Schmieder, P.; Domke, T.; Norris, D. G.; Kurz, M.; Kessler, H.; Leibfritz, D. Editing of
27 multiplicity in two- and three-dimensional heteronuclear NMR spectroscopy by Fourier transformation
28 of the pulse-angle dependency. *J. Magn. Reson.* **1991**, *93*, 430-435.
29
30 (38) Cicero, D. O.; Barbato, G.; Bazzo, R. Sensitivity enhancement of a two-dimensional experiment
31 for the measurement of heteronuclear long-range coupling constants, by a new scheme of coherence
32 selection by gradients. *J. Magn. Reson.* **2001**, *148*, 209-213.
33
34 (39) Sousa da Silva, A. W.; Vranken, W. F. ACPYPE - AnteChamber PYthon Parser interfacE. *BMC*
35 *Res. Notes* **2012**, *5*, 367-367.
36
37
38
39
40
41
42
43
44
45
46
47
48
49
50
51
52
53
54
55
56
57
58
59
60

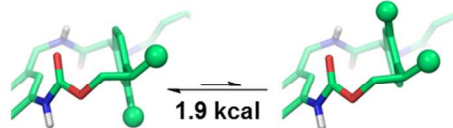
1
2
3
4
5
6
7
8
9
10
11
12
13
14
15
16
17
18
19
20
21
22
23
24
25
26
27
28
29
30
31
32
33
34
35
36
37
38
39
40
41
42
43
44
45
46
47
48
49
50
51
52
53
54
55
56
57
58
59
60

TABLE OF CONTENTS GRAPHIC



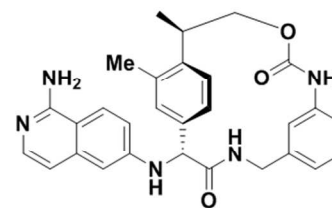
Atropisomerism due to macrocyclization

Design of Conformational Constraint



C-3 down
Desired

C-3 up



Single, desired atropisomer
16-fold increased TF/FVIIa inhibition